Rhizobiales commensal bacteria promote *Arabidopsis thaliana* root growth via host sulfated peptide pathway

Jana Hucklenbroich[1], Tamara Gigolashvili[2], Anna Koprivova[2], Philipp Spohr[3], Mahnaz Nezamivand Chegini[2,4], Gunnar W. Klau[3], Stanislav Kopriva[2], Ryohei Thomas Nakano[1,#]

[1]Department of Plant Microbe Interactions, Max Planck Institute for Plant Breeding Research, Cologne, Germany

[2]Institute for Plant Sciences, Cluster of Excellence on Plant Sciences (CEPLAS), University of Cologne, Cologne, Germany

[3]Algorithmic Bioinformatics, Cluster of Excellence on Plant Sciences (CEPLAS), Heinrich Heine University, Düsseldorf, Germany

[4]Institute of biotechnology, Shiraz university, Shiraz, Iran

[#]Corresponding author: nakano@mpipz.mpg.de

Short title:

Root manipulation by commensal bacteria

Abstract

Root-associated commensal bacteria that belong to the order Rhizobiales, which also contains symbiotic and pathogenic bacteria, promote primary root growth of *Arabidopsis thaliana*. Yet, its underlying molecular mechanism and physiological impact remained unclear. Here, we conducted a transcriptomic analysis of *A. thaliana* roots inoculated with root-associated commensal bacteria of Rhizobiales and sister lineages and revealed common and strain/lineage-specific transcriptional responsea, possibly mediated by WRKY and ANAC family of transcription factors. We revealed that the observed common response was also partially triggered by a wide range of non-pathogenic bacteria, fungi, and a multi-kingdom synthetic community (SynCom). This response was characterized by a down-regulation of genes related to intracellular redox regulation, suggesting distinctive redox status between pathogenic and non-pathogenic interactions. By integrating this analysis with developmental and cell biological analyses, we identified a crucial role for the sulfated peptide pathway mediated by TYROSYLPROTEIN SULFOTRANSFERASE (TPST) in Rhizobiales root growth promotion (RGP) activity. Conversely, none of the known sulfated peptide pathway appeared to be required for this activity, suggesting a novel sulfated protein pathway targeted by Rhizobiales RGP. Finally, we show that TPST is needed for RGP exerted by Rhizobiales but not Pseudomonadales isolates, delineating lineage-specific mechanisms to manipulate host root development.

Introduction

Various prokaryotic and eukaryotic microorganisms heavily colonize plant tissues in nature, collectively shaping the plant microbiota. Many of these do not engage in pathogenic or mutually symbiotic lifestyles, and are therefore frequently referred to as "commensal" microbes (Berg et al., 2020). Bacterial communities associated with roots (root bacterial microbiota) are significantly distinct from soil microbiota (Bulgarelli et al., 2012; Lundberg et al., 2013) and qualitatively highly conserved across different plant species at the family level (Hacquard et al., 2015; Thiergart et al., 2020). At the quantitative and strain levels, however, there appears to be host species/genotype specificity (Wagner et al., 2016; Zgadzaj et al., 2016; Wippel et al., 2021; Yu et al., 2021). These findings indicate the existence of a regulatory mechanism in plant and bacteria that enables taxonomically defined community assembly in a host-dependent manner. It also implies that, over the course of evolution, the extant microbiota

members have benefited the host plants and *vice versa*. Recent studies have provided evidence that the root bacterial microbiota as a community is vital for plant health, for example, by protecting the host from fungi (Wei et al., 2015; Duran et al., 2018) or by facilitating nutrient acquisition (Castrillo et al., 2017; Harbort et al., 2020; Salas-Gonzalez et al., 2021). Imbalance of the microbiota compositions ("dysbiosis") in roots as well as in leaves results in growth penalty (Chen et al., 2020; Finkel et al., 2020), illustrating the importance of eubiotic homeostasis of root microbiota (Paasch and He, 2021). Moreover, root bacterial microbiota members can interfere with root development and immunity. For example, many if not all commensal bacteria isolated from healthy *A. thaliana* roots are capable of either promoting or inhibiting host primary root growth in mono-association (Finkel et al., 2020). Another subset of root commensals have been shown to suppress root growth inhibition triggered by a chronic exposure to flg22, a 22-amino acid immunogenic peptide derived from bacterial flagella (thereby referred to as suppressive isolates)(Gomez-Gomez et al., 1999; Garrido-Oter et al., 2018; Yu et al., 2019; Ma et al., 2021; Teixeira et al., 2021). Overall, these studies have demonstrated the holobiome concept, an idea of collectively considering plants and associated microbiota as a single physiological and ecological unit. In contrast, our knowledge about the physiology of plants, including developmental regulation of roots, has been primarily provided by the studies using axenic plants. Toward ultimate understanding of the plant molecular physiology under ecological conditions, it remains necessary to better understand the molecular dialog between plants and commensal bacteria and how this influences host physiological pathways.

Comparative analysis of root microbiota across a wide range of plant species has identified bacterial lineages that are highly prevalent across and abundant within root microbiota (Hacquard et al., 2015). These include Rhizobiales, which is a bacterial order within the class Alphaproteobacteria, containing strains that engage in different lifestyles. Bacterial species in the order Rhizobiales include rhizobia, a paraphyletic group of bacteria that induce nodule organogenesis in legume roots and fix atmospheric nitrogen into ammonium for the host growth, and Agrobacterium, a monophyletic group of bacteria within the genus *Rhizobium* that invade plant tissues to induce tumors and ultimately restrict plant growth. These lifestyles are highly differentiated and require dedicated genes in bacteria and plants, such as *nod* and *nif* genes in rhizobia, *vir* genes in Agrobacterium, and *NOD FACTOR RECEPTOR* (*NFR*)

genes in legumes. The vast majority of Rhizobiales order bacteria, including strains that were isolated from soil or animals and therefore do not directly engage in interaction with plant hosts, do not possess these genes (Garrido-Oter et al., 2018). A recent study showed that host-associated and soil free-living lifestyles are frequently interchangeable (Wang et al., 2020). We previously showed that the extant commensal Rhizobiales bacteria are commonly capable of promoting primary root growth of *Arabidopsis thaliana* Col-0 wild-type plants when gnotobiotically inoculated with germ-free hosts. Bacterial isolates from the sister lineages, Sphingomonadales and Caulobacterales, did not possess this host root growth promotion (RGP) activity, implying that the RGP activity represents an ancestral trait specific to the order Rhizobiales (Garrido-Oter et al., 2018). The wide prevalence among extant Rhizobiales strains also suggests an important role of the RGP activity in interaction between *A. thaliana* roots and Rhizobiales commensals. Therefore, revealing the molecular mechanisms by which Rhizobiales bacteria interfere with host root growth may provide a valuable insight into the root-commensal molecular dialog.

In the previous study, we showed that Rhizobiales RGP was associated with an enlargement of the root meristematic zone (MZ), where cells undergo proliferation without elongation or differentiation, while the cell size in the elongation zone (EZ) and the differentiation zone (DZ) was comparable between axenic and R129_E-inocualted roots (Garrido-Oter et al., 2018). Root cell growth and proliferation are regulated by an orchestrated operation of various pathways: The mitotic activity of stem cell daughters within the MZ is maintained by a gradient accumulation of PLEHTHORA (PLT) transcription factors (TFs) under the control of auxin (Aida et al., 2004; Galinha et al., 2007). Auxin accumulated within the MZ induces expression of *TYROSYLPROTEIN SULFOTRANSFERASE* (*TPST*), which encodes an enzyme to catalyze protein sulfation of proteins (Komori et al., 2009; Zhou et al., 2010), including ROOT MERISTEM GROWTH FACTOR (RGFs) (Matsuzaki et al., 2010; Shinohara, 2021). Recent studies showed that perception of RGFs lead to activation of MITOGEN-ACTIVATED PROTEIN (MAP) kinases and redistribution of reactive oxygen species (ROS) to increase the PLT protein accumulation (Lu et al., 2020; Shao et al., 2020; Yamada et al., 2020). Accumulation of auxin and PLT gradually decreases along with the longitudinal axis of the roots and an auxin minimum is formed at the transition zone (TZ) where cytokinin antagonizes with auxin to switch cell fate from division to elongation (Dello Ioio et al., 2008; Di Mambro et al., 2017). This transition

process is also influenced by brassinosteroid and ROS distribution (Tsukagoshi et al., 2010; Chaiwanon and Wang, 2015). After the cell fate transition, the root cells continue growing within the EZ until they reach to the DZ. This elongation in the EZ is facilitated by gibberellin and another group of sulfated peptides, PHYTOSULFOKINE (PSK) and PLANT PEPTIDE CONTAINING SULFATED TYROSINE 1 (PSY1) (Matsubayashi et al., 2006; Amano et al., 2007; Achard et al., 2009; Ubeda-Tomas et al., 2009; Ladwig et al., 2015), whose sulfation is also dependent on TPST (Komori et al., 2009). The *tpst* mutant of *A. thaliana* lacks all functional sulfated peptides, including but not limited to RGFs, PSKs, and PSY1, as well as another class of sulfated peptides involved in endodermal cell differentiation (CASPARIAN STRIP INTEGRITY FACTOR, CIFs; Doblas et al., 2017), shows a highly disorganized root MZ and therefore exhibits severe root growth defects, showing the crucial role of the sulfate peptides in root growth regulation (Komori et al., 2009). It is plausible that Rhizobiales commensal bacteria target one of the aforementioned processes that coordinately dictate the primary root growth to exert the RGP activity. Yet, its underlying molecular mechanism is unknown. Our previous study showed that genetic perturbation of auxin-cytokinin antagonism in *arr1arr12* and *ahk3-3* mutants (Dello Ioio et al., 2008) did not disrupt Rhizobiales RGP (Garrido-Oter et al., 2018), pointing to a possible role of other components than auxin and cytokinin.

In this study, to disentangle the molecular interactions between *A. thaliana* and commensal Rhizobiales, we examined the host transcriptional response in roots inoculated with Rhizobiales and sister lineage commensal isolates. We identified common transcriptional responses commonly triggered by these bacteria. We revealed that a part of the observed common response was also triggered by a wide range of non-pathogenic bacterial and fungal microbes. By analyzing linage-specific responses and the developmental details of roots inoculated with Rhizobiales, we show that TPST, but none of the known receptors for RGF and PSKs, is indispensable for Rhizobiales RGP. Lastly, we show that many Rhizobiales but not Pseudomonadales commensals require the TPST pathway to promote root growth, illuminating the lineage-specific innovation of mechanisms to interfere with the host root development.

157 **Results**

158 *Host transcriptional reprogramming by root-associated Alphaproteobacteria*
159 *commensals*

160 To obtain an overview of transcriptional responses to Rhizobiales commensals, we
161 isolated and sequenced RNA from *A. thaliana* (Col-0 wild type) roots inoculated with
162 a panel of root-associated commensals that belong to the class Alphaproteobacteria.
163 Our previous RNAseq analysis revealed that the transcriptional responses triggered
164 by R129_E were similar in roots at 4, 8, and 12 days post-inoculation (dpi), which were
165 largely different from roots at 16 dpi (Garrido-Oter et al., 2018). A statistically
166 insignificant or marginal RGP phenotype is typically observed at 12 dpi at the level of
167 primary root length, while developmental manipulation at the cellular level (i.e.
168 enlarged root MZ) already initiates at an earlier time point (at 4-8 dpi). Therefore, we
169 decided to harvest roots at 12 dpi for our RNA-seq experiment to consider the impact
170 of Rhizobiales RGP at the cellular level while minimizing the difference accounted for
171 by different root growth. As inoculant bacteria, we used R129_E, R13_A, Root491,
172 and Root142 from the order Rhizobiales and Root1497 and Root700 from sister
173 lineages Sphingomonadales and Caulobacterales, respectively, as an outgroup
174 control. Among these isolates, only Rhizobiales strains exhibit root growth promotion
175 (RGP) activity, while only R129_E and Root1497 are able to suppress host flg22-
176 triggered root growth inhibition (Garrido-Oter et al., 2018). We identified a total of 1,439
177 differentially expressed genes (DEGs) between axenic and commensal-inoculated
178 roots, based on the false discovery rate (FDR; $\alpha = 0.05$) and $\log_2$-scale fold changes
179 ($|\log FC| > 1$), and a principal coordinates analysis (PCoA) was performed using their
180 zero-centered expression values (Figure 1A). This revealed that these commensals
181 triggered a significant shift in the host transcriptional profiles ($R^2 = 0.662$, $P < 0.001$,
182 PERMANOVA) in a manner dependent on the taxonomic lineages they belonged to
183 (filled *versus* open shapes; $R^2 = 0.457$, $P = 0.0045$, pairwise PERMANOVA between
184 Rhizobiales and sister lineage isolates). We revealed a number of DEGs specific to
185 each inoculation, as well as DEGs commonly identified in more than one inoculation
186 (Supplemental Figure 1). On the other hand, transcriptional responses to these
187 commensal bacteria were qualitatively similar and showed a strong correlation
188 (Figures 1B and 1C), indicating that the taxonomy-dependency of host transcriptional
189 reprogramming, as shown in Figure 1A, is explained by their quantitative differences.

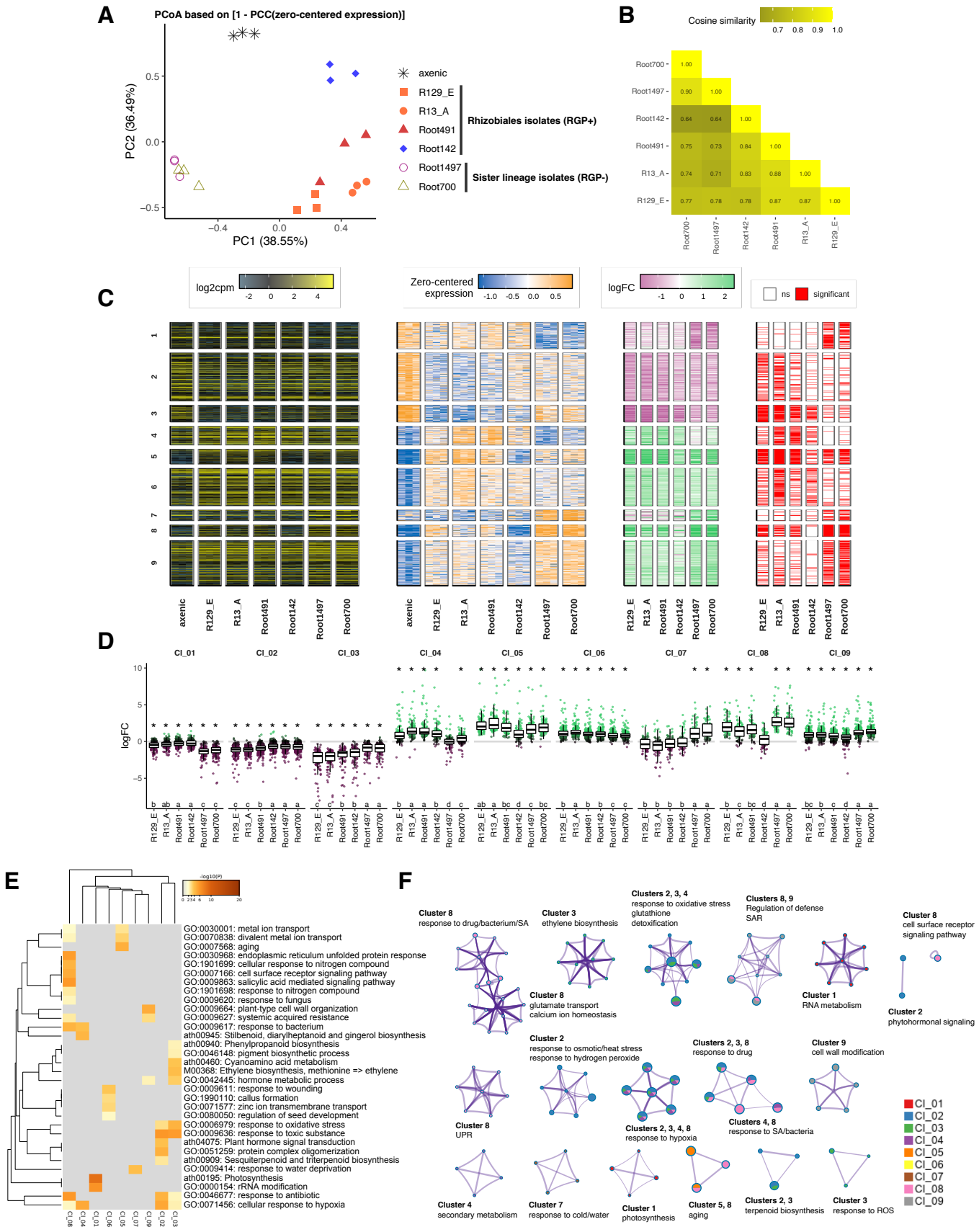

Figure 1. Alphaproteobacteria commensals trigger qualitatively similar transcriptional responses in host roots.
(A) A principal coordinates analysis separated transcriptome of axenic roots (asterisks), roots inoculated with Rhizobiales commensals (closed shapes), and roots inoculated with sister lineage isolates (open shapes). (B) A heatmap showing cosine similarities between logFC upon Alphaproteobacteria commensal inoculations. (C) Heatmaps showing $\log_2$-scale count per million (log2cpm), zero-centered expression values, $\log_2$-scale fold changes (logFC), and significance (FDR < 0.05; |logFC| > 1), aligned according to their k-means cluster assignment (k = 9, based on Bayesian information criterion). (D) Boxplots showing logFC of each k-means cluster. Asterisks indicate statistical significance corresponding to Student's one-sample t test after Bonferroni's correction for multiple comparisons (μ = 0; α = 0.001) and letters indicate statistical significance corresponding to pairwise Wilcoxon's rank sum test after Bonferroni's correction for multiple comparisons within each cluster (α = 0.05). (E) A heatmap showing enrichment of GO terms in the *k*-means clusters. (F) A network plot of enriched GO terms. Each node represents each GO term, and GOs with overlapping gene contents are connected with edges. *k*-means assignment of composing genes is shown as a pie chart. We selected the terms with the best *P* values from each of the 9 clusters, with the constraint that there are no more than 15 terms per cluster and no more than 250 terms in total. Representative terms are manually curated and indicated with composing *k*-means clusters for each GO cluster.

190 To obtain functional insights, we classified all 1,439 DEGs into nine *k*-means
191 gene clusters based on the zero-centered expression values and tested whether Gene
192 Ontology (GO) categories were enriched in each cluster (Figures 1C to 1F and
193 Supplemental Figure 2). We assigned down-regulated genes into Clusters 1, 2, and 3
194 and up-regulated genes into Clusters 4 to 9. Clusters 2 and 5 illustrated the general
195 response to these commensal bacteria, and Clusters 3, 4, and 6, and Clusters 1, 7,
196 and 9 represented responses quantitatively characteristic to Rhizobiales and sister
197 lineage isolates, respectively. The commonly up-regulated Cluster 5 was enriched in
198 genes related to metal ion transport and ageing, while commonly down-regulated
199 Cluster 2 was enriched in genes related to response to hypoxia and to various abiotic
200 stresses, as well as genes associated with biosynthesis of terpenoid, phytohormone
201 signal transduction, and the detoxification pathway. Clusters characteristic to sister
202 lineage isolates (Clusters 1, 7, and 9) were enriched in unique GO categories, such
203 as photosynthesis (Cluster 1), response to cold and water deprivation (Cluster 7), and
204 cell wall rearrangement and immune responses (Cluster 9). Clusters characteristic to
205 Rhizobiales were characterized by up- and down-regulation of "Response to hypoxia"
206 and "detoxification" (Clusters 3 and 4), down-regulation of biosynthesis of ethylene,
207 glucosinolate, and flavonoid, and response to various abiotic stresses (Cluster 3), and
208 up-regulation of response bacteria, wounding, salicylic acid (SA), and jasmonic acid
209 (JA) (Clusters 4 and 6). Cluster 8 contained genes up-regulated by all isolates except
210 for Root142, which were enriched in immune-related genes, such as genes
211 responding to SA, bacteria, fungi, and hypoxia or related to calcium homeostasis, as
212 well as genes involved in response to abiotic stresses such as heat, drugs, and amino
213 acids. We previously reported that Root142 is one of the Rhizobiales strains that were
214 able to efficiently colonize *A. thaliana* roots (Garrido-Oter et al., 2018), implying the
215 ability of Root142 to partly evade recognition by the host or to interfere with these host
216 immune responses, albeit its inability to suppress flg22-triggered root growth inhibition.
217 In contrast, only a handful (4 up- and 6 down-regulated genes) of DEGs were found
218 to be common between suppressive R129_E and Root1497 (Supplemental Figure 1),
219 probably accounted for by different mechanisms employed by these isolates to
220 interfere with host immune responses. These findings illustrate that the tested
221 Alphaproteobacteria commensals commonly interfere with the host genetic pathways
222 associated with hypoxia, detoxification, and plant immunity, to a different extent
223 depending on the isolates. Lineage-specific DEGs (46 and 99 genes specific to

224 Rhizobiales and the sister lineage, respectively) and isolate-specific DEGs (from 44 to
225 164 genes) also demonstrated the presence of lineage/strain-specific responses,
226 whose functional aspects remained unclear based on their GO annotation.
227 We then looked for TF binding motifs enriched in the 1-kb upstream sequences
228 of the genes in each cluster. We identified several binding motifs, mainly from the TF
229 families of WRKY and ANAC, as well as the AHL family of DNA-binding proteins
230 (Figure 2A), suggesting a role of these TF families in commensal-triggered
231 transcriptional reprogramming. We found that 20 WRKY and NAC family TFs were
232 differentially expressed (differentially expressed TFs, DETFs), and used these DETFs
233 as a list of potential regulators to infer a gene regulatory network (GRN) by the so-
234 called GENIE3 algorithm (Figure 2B). This algorithm considers both positive and
235 negative potential regulations to infer a GRN, which is a strong advantage over
236 correlation-based approaches, such as *k*-means clustering and gene co-expression
237 networks (Huynh-Thu et al., 2010). The inferred GRN was composed of two arbitrarily
238 defined modules, characterized by the predominance of either WRKY or NAC family
239 DETFs as hub nodes (module 1 and module 2, respectively; Figure 2B). Among
240 DETFs, WRKY54 and ANAC060 showed the first and second highest centrality
241 indices (degree, closeness, and betweenness centralities), suggesting their role in the
242 observed transcriptional reprogramming. Genes commonly induced/suppressed by
243 Alphaproteobacteria commensals (Clusters 1, 8, and 9) were enriched in module 1,
244 whereas genes in the Rhizobiales-characteristic clusters (Clusters 3, 4, ad 6) were
245 enriched in module 2 (Supplemental Figures 3A and 3B). We observed similar trends
246 using all DETFs, independent of promoter motif enrichment analysis, as potential
247 regulators to infer a GRN, albeit with a less clear GRN structure (Supplemental Figure
248 4). Importantly, in both GRNs, WRKY54 and ANAC060 were identified as candidate
249 hub regulators based on the centrality indices and connected with genes whose
250 transcriptional responses were commonly triggered by all isolates or characteristically
251 by Rhizobiales isolates, respectively. Together, our RNAseq experiments
252 demonstrated common and lineage-specific transcriptional responses in roots that
253 were potentially mediated by WRKY54 and ANAC060, respectively, along with other
254 TFs.
255
256
257

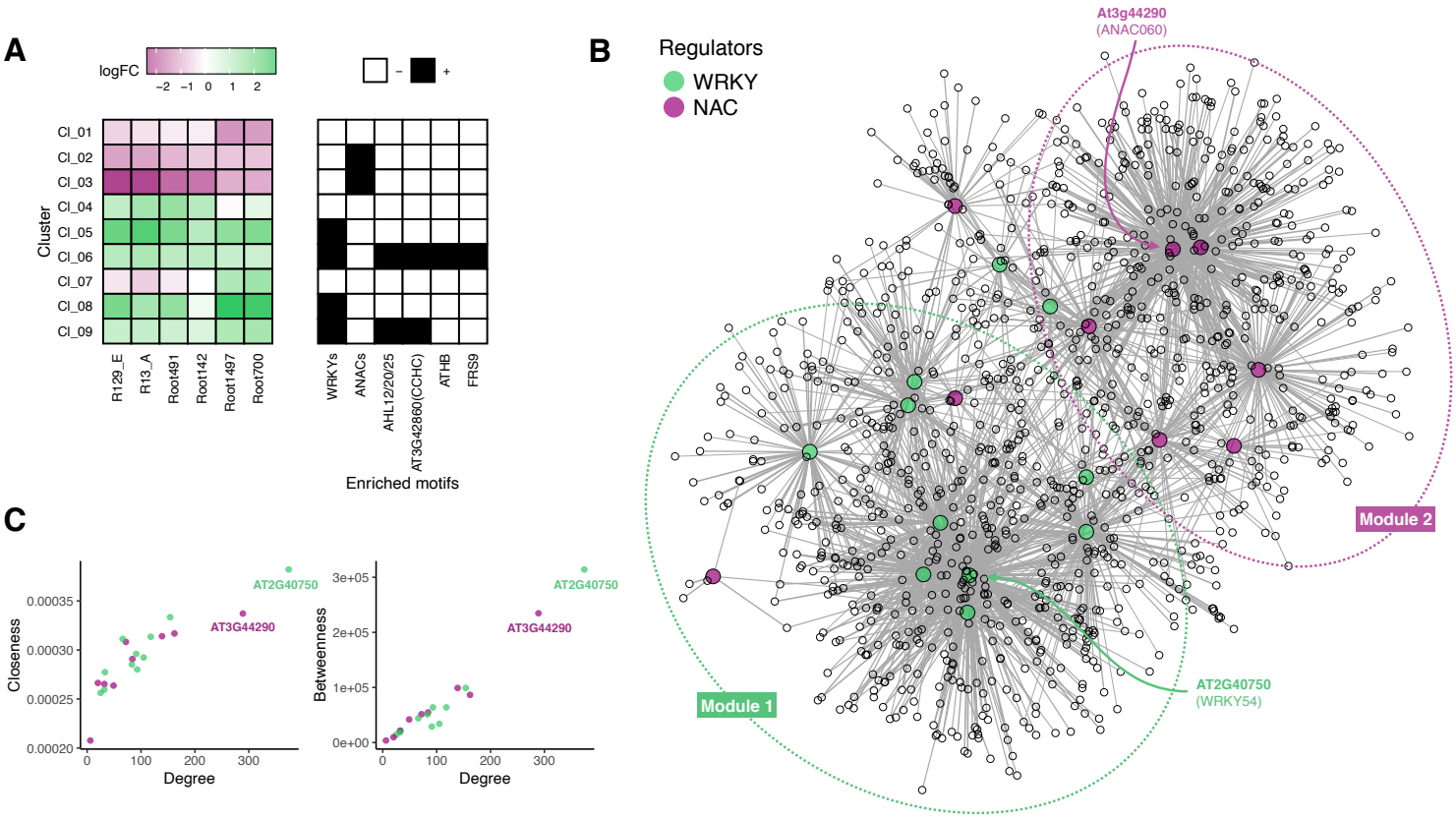

Figure 2. WRKY and ANAC transcription factors are important for transcriptional reprogramming.
(A) Heatmaps showing mean logFC of each cluster (left) and the enrichment of corresponding transcription factor binding motifs in their promoter regions (1-kb upstream from transcription initiation sites). AHL, AT-HOOK MOTIF CONTAINING NUCLEAR LOCALIZED; CCHC, CCHC-type zinc-finger motif containing protein; ATHB, ARABIDOPSIS THALIANA HOMEOBOX; FRS9, FAR1-RELATED SEQUENCE9. (B) GENIE3-inferred gene regulatory network using WRKY (green) and ANAC (magenta) family DETFs as potential regulators (colored; bigger node size). Arbitrarily defined modules are shown by dotted lines. (C) Degree, closeness, and betweenness centralities were computed based on the network in (B) for all potential regulators. Green and magenta dots correspond to WRKY and ANAC family TFs.

258 *Overlapping transcriptional responses to a wide range of non-pathogenic microbes*
259 Our RNAseq experiments identified common as well as lineage-specific transcriptional
260 responses, both of which were enriched in similar GO terms, such as "detoxification"
261 and "response to hypoxia". We noted that these GO terms were also found among
262 genes responding to other root microbiota members (Hacquard et al., 2016; Ma et al.,
263 2021; Teixeira et al., 2021; Wippel et al., 2021). This suggests that a wide range of
264 root-associated microbes might broadly interfere with this response, and we aimed to
265 understand the extent to which the observed root transcriptional response is common
266 and specific to Alphaproteobacteria and Rhizobiales commensals. We compared our
267 data with publicly available transcriptomic datasets using the roots inoculated with
268 root-inhabiting microbes that engage in beneficial, commensal, and pathogenic
269 lifestyles under different nutrient conditions, in different experimental setups, at
270 different time points (Supplemental Table 1). These include beneficial and pathogenic
271 *Colletotrichum* fungi (*C. tofieldiae* and *C. incanum*; Hacquard et al., 2016; Hiruma et
272 al., 2016), a bacterial synthetic community (B-SynCom; Harbort et al., 2020), and a
273 multi-kingdom synthetic community (SynCom) composed of bacteria, fungi, and
274 oomycetes (BFO-SynCom; Hou et al., 2020). In addition, we sequenced RNA obtained
275 from roots inoculated with beneficial and pathogenic *Burkholderia* bacteria (*B.*
276 *phytofirmans* and *B. glumae* isolated from onion and rice, respectively), as well as
277 from roots inoculated with R129_E in the presence or absence of flg22 to consider the
278 impact of host immune responses. We compared and clustered responses to different
279 microbial inoculations based on the similarity of logFC (Figures 3A). LogFC within non-
280 pathogenic inoculations exhibited significantly greater similarities than between the
281 responses to pathogenic and non-pathogenic inoculations (Figure 3B), without any
282 clear sign of the taxonomy or the complexity of respective inocula (shapes in the
283 dendrogram). A PCoA based on the transcriptome-wide logFC similarities revealed a
284 clustering of non-pathogenic inoculations, irrespective of their taxonomy and
285 complexity (Figure 3C). A pairwise PERMANOVA between different lifestyles
286 (commensal, beneficial, pathogenic, and SynCom) revealed that all combinations of
287 lifestyles significantly contribute to the difference in the host transcriptional responses
288 (FDR-corrected P values of 0.002 ~ 0.01), while the R^2 values were larger between
289 pathogenic and non-pathogenic lifestyles than within non-pathogenic lifestyles
290 (Supplemental Table 2). Notably, minimizing batch effects by a canonical analysis of

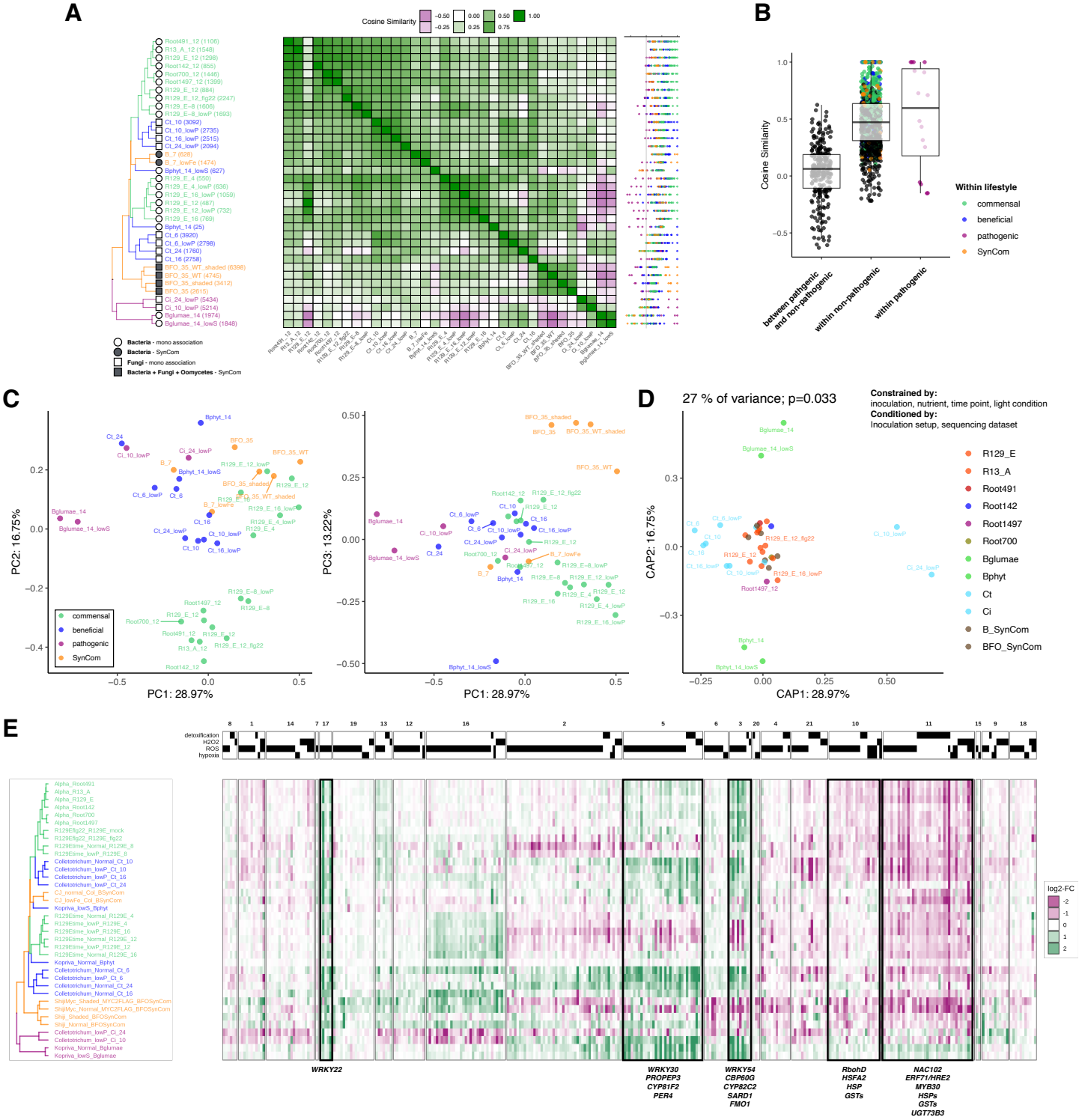

Figure 3. Non-pathogenic microbial inoculation triggered similar transcriptional responses in the host roots.
(A) A heatmap showing cosine similarities between logFC upon different microbial inoculations. DEGs were selected based on the inoculation in rows (numbers of DEGs are shown in parentheses), whose logFC cosine similarity was calculated in comparison with inoculations in columns. For each row, all cosine similarity values were plotted on the right, whose colors indicate the lifestyle of the comparing inoculation. (B) Cosine similarities within non-pathogenic inoculations and within pathogenic inoculations were higher than those between pathogenic and non-pathogenic inoculations. (C) Principal coordinates analysis based on logFC cosine similarities of all commonly quantified genes (n = 21,815). Colors correspond to lifestyles. (D) Constrained analysis of principal coordinates (CAP) based on the logFC cosine similarities, using the constraining and conditioning factors indicated above. Colors correspond to inoculated microbial strains. (E) A heatmap showing logFC of genes assigned with the GO categories related to detoxification and response to hydrogen peroxide, reactive oxygen species, and hypoxia. Inoculations are aligned according to the dendrogram in (A) and genes are aligned according to k-means clustering as shown in Supplemental Figure 2B. Numbers indicated in the names of inoculation indicate the time point of harvesting (dpi).

291 principal coordinates (CAP) clustered all non-pathogenic interactions with microbes
292 isolated from *A. thaliana* (Figure 3D).
293 Concatenated lists of DEGs (13,889 genes in total) were then classified into 21
294 *k*-means clusters and tested for their enriched GO categories (Supplemental Figures
295 5A and 5B). This identified the detoxification pathway to be strongly enriched in Cluster
296 11 (P = 5.1×10^{-18}), whose transcriptional suppression characterized the non-
297 pathogenic interactions. Our of 22 genes in Cluster 11 assigned with the GO term
298 "detoxification", 13 genes encode glutathione (GSH) *S*-transferases (GSTs), which
299 play an important role in cellular redox homeostasis. The hypoxia response is known
300 to trigger ROS production via RESPIRATORY BURST OXIDASE HOMOLOG D
301 (RbohD) in *A. thaliana* (Pucciariello et al., 2012), and is associated with strong immune
302 response induction. Therefore, we speculated that non-pathogenic interactions may
303 impact the root redox response. Among DEGs, we found a total of 327 genes assigned
304 with GO categories of response to hypoxia, response to ROS, and detoxification
305 pathway (Figure 3E). The hypoxia-triggered immune response includes transcriptional
306 up-regulation of genes crucial for plant immunity, such as *FLAVIN-DEPENDENT*
307 *MONOOXYGENASE 1* (*FMO1*; (Hartmann et al., 2018), *CALMODULIN-BINDING*
308 *PROTEIN 60-LIKE G* (*CBP60G*; (Wang et al., 2009), *ELICITOR PEPTIDE 3*
309 *PRECURSOR* (*PROPEP3*; (Huffaker and Ryan, 2007), *CYTOCHROME P450*
310 *FAMILY 82, SUBFAMILY C, POLYPEPTIDE 2* (*CYP82C2*; (Rajniak et al., 2015), and
311 *PEROXIDASE4* (*PER4*; (Rasul et al., 2012), in a WRKY22-dependent manner (Hsu
312 et al., 2013). In our meta-analysis, these genes were mostly up-regulated in many
313 pathogenic and non-pathogenic interactions (Clusters 3/5/17), suggesting that the
314 genetic sector responding to commensal bacteria inoculation overlaps with the
315 hypoxia response. On the other hand, another subset of hypoxia-responsive genes,
316 such as *RbohD*, *HEAT SHOCK TRANSCRIPTION FACTOR A 2* (*HSFA2*),
317 *ARABIDOPSIS NAC DOMAIN CONTAINING PROTEIN 102* (*ANAC102*), and
318 *HYPOXIA RESPONSIVE ERF2* (*HRE2*), along with many *GST* genes, were found in
319 Cluster 11 and down-regulated by non-pathogenic microbes. Down-regulation of the
320 transcriptional levels of *GST*s was not limited to a subset of isoforms but broadly
321 observed across most of the *GST* genes encoded by the *A. thaliana* genome
322 (Supplemental Figure 5C), suggesting a link to the general redox response rather than
323 a specific secondary metabolic pathway (discussed below). Overall, these results
324 suggest that the host root redox status linked with the expression of genes related to

325 response to hypoxia and the detoxification pathway is associated with different types
326 of interactions between pathogenic and non-pathogenic microbe, rather than the
327 Rhizobiales- or Alphaproteobacteria-specific responses.
328
329 *ANAC060 transcription factor characterized Rhizobiales-specific root transcriptional*
330 *response*
331 Our initial RNAseq experiment identified the hypoxia response and detoxification
332 pathway in the genes enriched in Rhizobiales-characteristic gene clusters (Clusters 3
333 and 4 in Figure 1), while the subsequent meta-analysis revealed that these gene
334 pathways were rather associated with interaction with a wide range of microbes.
335 Clusters 3, 11, and 17 contained more than 40% of Alphaproteobacteria DEGs
336 (Supplemental Figure 5A, rank abundance plot) and contained genes related to
337 hypoxia-responsive immunity and detoxification pathways (Figure 3E), suggesting that
338 the hypoxia response and detoxification pathways are not necessarily associated with
339 the Rhizobiales RGP activity. In order to characterize the molecular mechanism
340 responsible for Rhizobiales-triggered RGP, we aimed to further explore the response
341 characteristic to Rhizobiales independently of *k*-means clustering and Gene Ontology
342 annotations. Given the uncharacterized nature of interaction included in the meta-
343 analysis, we again focused on our dataset targeted to Alphaproteobacteria
344 commensals. We identified a total of 46 genes that were significantly up- or down-
345 regulated by Rhizobiales but not by sister lineage isolates ("Rhizobiales DEGs"; Figure
346 4A), which were then mapped onto the GRN shown in Figure 2B. We found that
347 Rhizobiales DEGs were exclusively located on a sub-module within module 2 and
348 tightly associated with *ANAC060* (Figures 4B and 4C and Supplemental Figure 3C).
349 Given that *ANAC060* is one of the two DETFs with the highest centralities (Figure 3C)
350 and the only TF among Rhizobiales DEGs (Figure 4A), we speculate that ANAC060
351 is crucial for the Rhizobiales-specific transcriptional response, a part of which
352 ultimately triggers RGP phenotype.
353
354 *Plant sulfated peptides are required for R129 E RGP*
355 We previously reported that the Rhizobiales RGP is associated with the enlargement
356 of and increased cell number within the root MZ, but not with cell size, pointing to
357 facilitated cell division triggered by Rhizobiales commensals. We confirmed this by
358 staining cells undergoing S-phase by a thymidine analog 5-ethynyl-2'-deoxyuridine

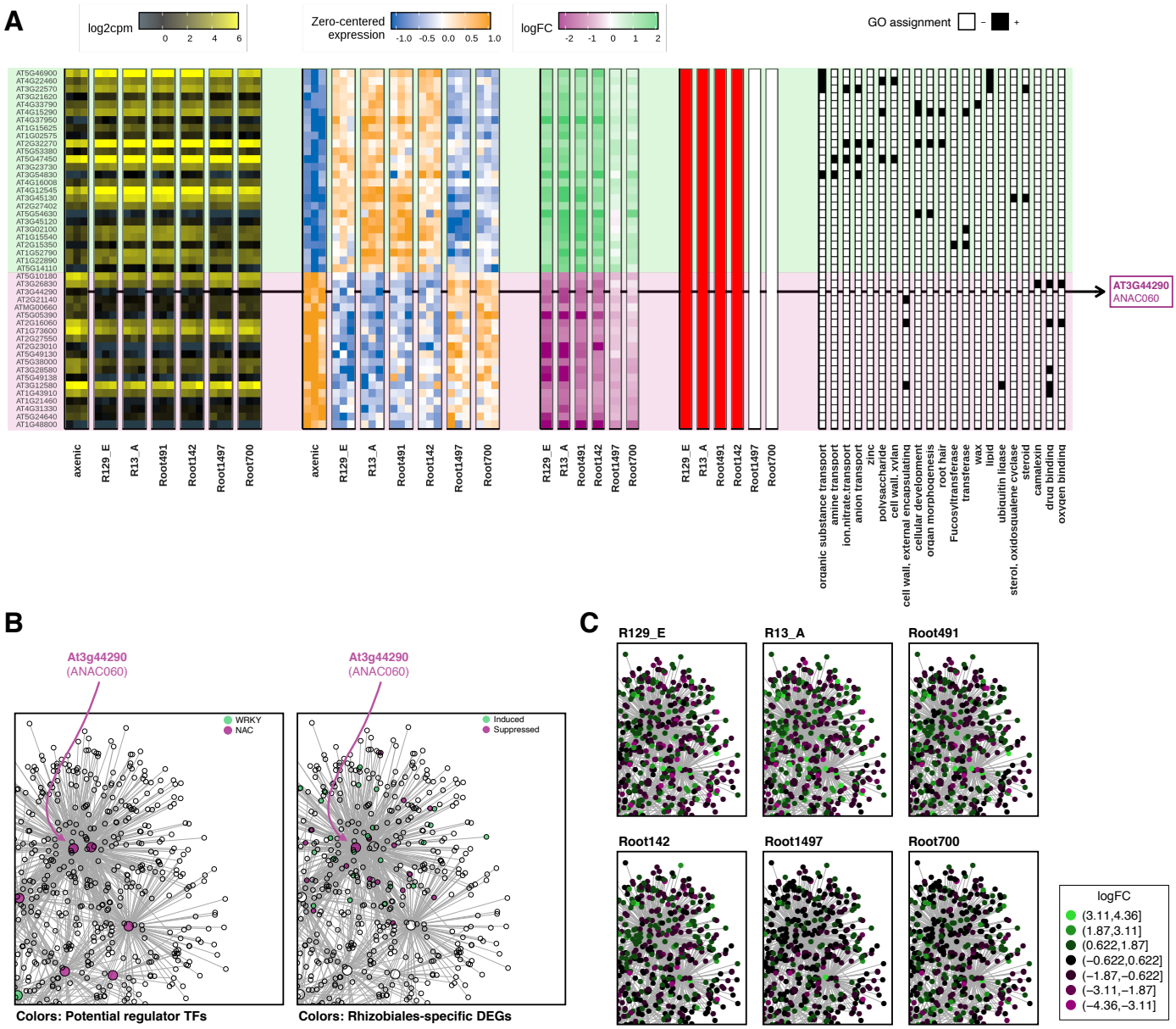

Figure 4. Rhizobiales-specific DEGs are potentially regulated by ANAC060.
(A) Heatmaps showing log2cpm, zero-centered expression values, logFC, significance, and GO assignment of genes specifically regulated by Rhizobiales commensals but not by sister lineage isolates. (B) Enlarged view of the GENIE3-inferred GRN, shown in Figure 2B, colored for potential regulator TFs (left) or Rhizobiales-specific DEGs (right). (C) Same view as in (B), colored by their logFC upon different bacterial inoculation.

359 (EdU; Supplemental Figure 7A). This corroborated the scenario that Rhizobiales RGP
360 targets root MZ homeostasis. On the other hand, we did not find a dramatic increase
361 or decrease of auxin and cytokinin, at least not at the detectable level of DR5:ER-GFP
362 and TCSn:ER-GFP accumulation (Supplemental Figures 7B and 7C), which further
363 supported the potential role of other components than auxin-cytokinin antagonism. In
364 published single-cell RNA sequencing (scRNA-seq) data of *A. thaliana* roots (Denyer
365 et al., 2019), *ANAC060* showed relatively high expression in the cell population
366 characterized by the expression of meristematic genes ("cluster 11"; Supplemental
367 Figures 6A and 6B). We also found that the top 100 genes co-expressed with
368 *ANAC060* across 4,727 sequenced root cells were enriched in the GO categories
369 related to root MZ regulation, such as "meristematic growth," "regulation of cell
370 division," and "response to gravity" (Supplemental Figure 6C). Interestingly, genes that
371 were best co-expressed with *ANAC060* in the scRNAseq dataset included *RGF3*
372 (14th), as well as *PLT1* (5th) and *PLT2* (63rd) (Supplemental Figures S6A). Moreover,
373 a pervious study reported that ANAC060 potentially represses the expression of PSY1
374 while activating the expression of PSY4, a sequence-related homologue of PSY1 (Yu
375 et al., 2020; Tost et al., 2021), overall suggesting a potential link between ANAC060
376 and the sulfated peptide pathway.

377 To test the link between Rhizobiales RGP and the plant sulfated peptide pathway,
378 we inoculated a Rhizobiales commensal R129_E with *tpst* mutant plants, depleted in
379 all classes of functional sulfated peptides. Strikingly, we identified a lack of the RGP
380 phenotype in the *tpst* mutant (Figure 5A), without a clear depletion of bacterial cells
381 from roots (Figure 5B). In contrast, we observed significant RGP in *rgi1;2;3;4;5-1*,
382 *pskr1pskr2psy1r*, and *sgn3* mutants, which are impaired in perception of RGF, PSK,
383 and CIF peptides, respectively (Figure 5C and Supplemental Figure 8A). Likewise, the
384 RGP activity of R129_E remained functional when the three major isoforms of RGF
385 peptides operating in the root MZ were genetically abolished in the *rgf123* mutant
386 (Supplemental Figure 8A) (Matsuzaki et al., 2010). Disorganized root MZ in the *tpst*
387 mutant is known to be rescued by external application of RGF1 peptide but not its
388 desulfated form (dRGF1). However, treatments with neither of these peptides rescued
389 the RGP activity of R129_E, despite the substantial recovery of root MZ under these
390 conditions (Supplemental Figures 8B and 8C). These findings demonstrate that
391 R129_E requires the host sulfotransferase enzyme TPST for its RGP activity but not
392 the RGF and PSK peptide pathways. Of note, the root MZ in the *rgi1;2;3;4;5* mutant

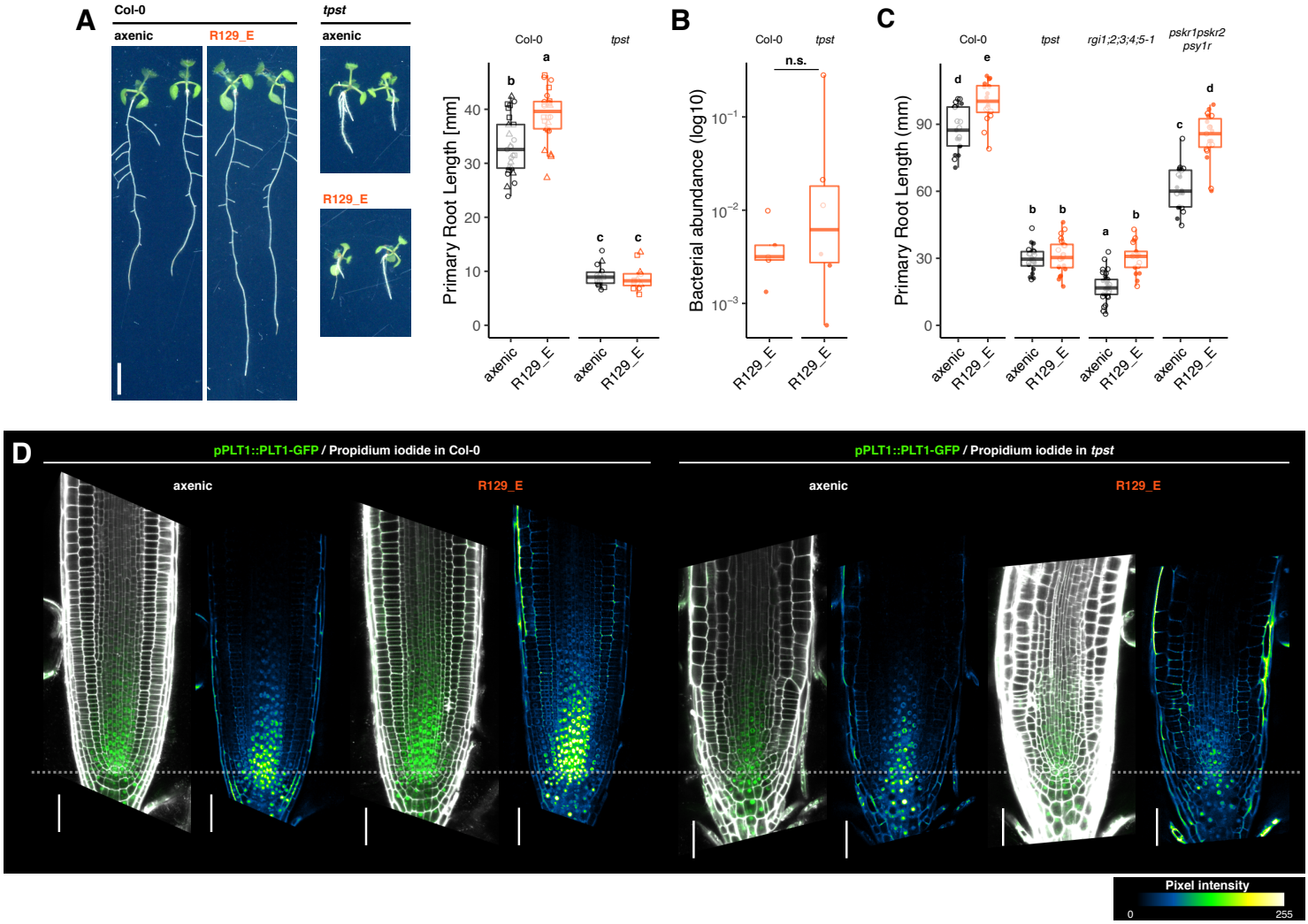

Figure 5. Plant sulfated peptide pathway is needed for R129_E RGP activity.
(A) Primary root growth and representative pictures of Col-0 and *tpst* plants grown axenically or inoculated with R129_E. Seeds were inoculated and grown under continuous light conditions for 12 days. (B) Bacterial abundance relative to plant biomass was quantified by DNA-based quantitative PCR using primers specific to *A. thaliana* and R129_E *16S rRNA* genes. No clear depletion of bacterial cells from *tpst* roots was observed. (C) Mutants impaired RGF1 perception (*rgi1;2,3;4;5-1*) or PSK perception (*pskr1pskr2psy1r*) did not phenocopy *tpst* when 7-day-old seedlings were inoculated with R129_E for 14 days under short-day conditions. (D) Col-0 root MZ accumulate higher amounts of proPLT1::PLT1-GFP when 7-day-old seedlings were inoculated with R129_E for 7 days under short-day conditions, whereas *tpst* root MZ accumulated a similar amount irrespective of R129_E inoculation. For each panel, a merged image of propidium iodide staining (gray) and PLT1-GFP (green) signals and an image only showing PLT1-GFP signals pseudo-colored as shown in the calibration bar are shown in left and right, respectively. Bars indicate 50 µm. Images are aligned with quiescent centers on the dotted line. Letters indicate statistical significance (α = 0.05) corresponding to Student's *t* test after fitting to a linear mixed model with biological and technical replicates as random factors, corrected for multiple comparison by the Benjamini-Hochberg method.

393 was even more severely disrupted than in the *tpst* mutant (Ou et al., 2016; Song et al.,
394 2016), while this mutant nonetheless exhibited the RGP activity when inoculated with
395 R129_E (Figure 5C). Combined with the observation that restoration of root MZ by
396 RGF1 did not rescue RGP activity, our findings point to a specific regulatory role for
397 sulfated peptides, making the potential confounding effects due to the pleiotropic effect
398 of highly disorganized root MZ in *tpst* less likely. Lastly, we inoculated wild-type and
399 *tpst* mutant plants expressing PLT1-GFP under its *cis*-regulatory sequence to test
400 whether R129_E showed any impact on PLT1 protein accumulation. This showed that
401 R129_E indeed stimulates the accumulation of PLT1-GFP in Col-0 root MZ, which was
402 not observed when the sulfated peptides were abolished in the *tpst* root MZ (Figure
403 5D). Overall, these findings indicate that the host sulfated peptide pathway is
404 indispensable for R129_E-stimulated accumulation of PLT1 protein, thereby
405 facilitating the cell division within the root MZ and promoting primary root growth.
406
407 *The sulfated peptide pathway is needed by Rhizobiales but not Pseudomonadales*
408 *RGP commensals*
409 We previously showed that the RGP activity is prevalent within the order Rhizobiales
410 (Garrido-Oter et al., 2018), while it remained unclear whether they promote root growth
411 by the same molecular mechanism. We, therefore, inoculated *tpst* mutants with two
412 additional Rhizobiales isolates, Root491 (*Agrobacterium*) and Root142
413 (*Sinorhizobium*), which were both used in the RNAseq analysis (Figure 1), and found
414 that none of these isolates were able to promote *tpst* mutant root growth (Figure 6A).
415 To further explore its prevalence, we inoculated *tpst* with a panel of Pseudomonadales
416 isolates, namely Root7, Root71, Root329, and Root569, which are also capable of
417 promoting *A. thaliana* root growth in a manner yet to be identified. Interestingly, these
418 isolates showed RGP activity even in the absence of the host TPST enzyme (Figure
419 6B). These findings indicate a specific and conserved contribution of the plant sulfated
420 peptide pathway to Rhizobiales RGP, but not Pseudomonadales RGP, illustrating the
421 clear distinction between these two RGP phenotypes at the molecular level. This also
422 implies that root-associated commensal bacteria have independently acquired RGP
423 capability more than once, pointing to a potential physiological relevance of this
424 phenotype in the context of plant-microbiota interactions.
425
426

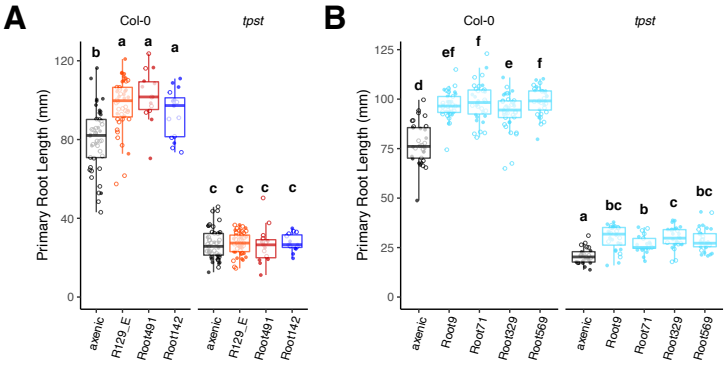

Figure 6. TPST is needed for the RGP activity explicitly exerted by Rhizobiales RGP but not Pseudomonadales.

Seven-day-old seedling of Col-0 and *tpst* were inoculated with a panel of Rhizobiales commensals (A) or Pseudomonadales commensals (B) and grown for 14 days under short-day conditions. Letters indicate statistical significance (α = 0.05) corresponding to Student's t test after fitting to a linear mixed model with biological and technical replicates as random factors, corrected for multiple comparison by the Benjamini-Hochberg method.

427 **Discussion**

428 *WRKY and ANAC family TFs in transcriptional responses to Alphaproteobacteria*
429 *commensals*

430 Our comparative transcriptomic analysis identified genes that were differentially
431 regulated by a panel of Alphaproteobacteria commensals. This enabled us to identify
432 common as well as strain/lineage-specific responses, which were qualitatively similar
433 and functionally overlapped with each other. The 1-kb upstream sequences of these
434 genes tend to possess binding motifs of WRKY and ANAC family TFs, suggesting the
435 role of these families of TFs in Alphaproteobacteria commensal-triggered
436 transcriptional reprograming. WRKY family TFs are widely known for their crucial role
437 in defense-related stress responses and are often also involved in plant development
438 such as leaf senescence (Phukan et al., 2016), while many ANAC family TFs are
439 reported to be involved in stress-induced regulation of development (Shao et al., 2015)
440 and also in plant immunity (Yuan et al., 2019). It is well known that the WRKY family
441 of TFs form a highly rigid transcriptional network (Eulgem and Somssich, 2007), and
442 disruption of a single gene is frequently insufficient for perturbation of the entire
443 network. This also appears to be the case for the ANAC family of TFs (Kim et al.,
444 2018), pointing to a complex transcriptional network that ultimately contribute to the
445 commensal-triggered reprogramming. The TF families identified in our promoter
446 enrichment analysis were also found in a recent study addressing the co-occurrence
447 of multiple TF binding motifs in the genes responding to immunogenic stimuli in roots
448 in a cell-type specific manner (Rich-Griffin et al., 2020), further supporting the idea of
449 their key role in plant-microbe interactions in roots of *A. thaliana*. A detailed time-
450 course transcriptomic analysis is needed to identify the key regulator of the entire
451 response and to test its contribution to the observed transcriptomic shift.

452

453 *Host redox status may play a role in the distinction between pathogenic and non-*
454 *pathogenic microbes*

455 Recent studies described transcriptional responses in roots and leaves to another set
456 of a panel of *A. thaliana* root- and leaf-derived bacterial commensals (Maier et al.,
457 2021; Nobori et al., 2021; Teixeira et al., 2021). These commensal bacteria triggered
458 qualitatively similar responses in the host, which is consistent with our finding that the
459 response to Alphaproteobacteria commensals were largely similar. Furthermore, we
460 have developed a method to compare transcriptional responses analyzed in

461 independent RNAseq experiments. This allowed us to identify a substantial overlap
462 between root transcriptional responses to a wide range of bacteria, fungi, and
463 SynComs, inoculated in very different experimental setups, expanding the model of
464 common transcriptional responses to a broader range of interactions. This includes
465 up-regulation of hypoxia-responsive immune-related genes by both pathogenic and
466 non-pathogenic interactions even after weeks of inoculation without causing growth
467 restriction. This is contradictory with the growth-defense tradeoff model, according to
468 which a chronic activation of immunity results in growth inhibition (Gomez-Gomez et
469 al., 1999; Huot et al., 2014), suggesting the presence of an immune response sector
470 that is uncoupled from the tradeoff. We also identified genes specifically and
471 commonly down-regulated by non-pathogenic microbes, which were enriched in the
472 detoxification pathway. We noted that this was mostly driven by the down-regulation
473 of genes encoding GSTs. GSTs are often involved in secondary metabolic pathways,
474 for example, by conjugation of GSH to toxic intermediates (thereby annotated as
475 detoxification pathway components). Moreover, GSH is one of the critical components
476 in sensing and regulating the cellular redox status, where GSTs play a crucial role
477 (Noctor et al., 2012). We observed that the down-regulation of GSTs was not limited
478 to GST isoforms that were specific to the family Brassicaceae (Supplemental Figure
479 5D, shaded by blue), which are often involved in lineage-specific secondary
480 metabolism (Dixon et al., 2010), but were broadly observed among different classes
481 of GSTs, including GSTUs and GSTFs (Pislewska-Bednarek et al., 2018). These
482 results point to a possibility that pathogenic and non-pathogenic microbes differentially
483 influence host cellular redox status. The broad impact on the expression of multiple
484 GST genes also implies that their transcriptional down-regulation may be a
485 consequence of altered GSH homeostasis, rather than a cause of the transcriptional
486 reprogramming. A recent study suggested that the extracellular and cytoplasmic ROS
487 responses are mutually distinguishable, where the cytoplasmic response is more
488 prolonged (Arnaud et al., 2021). GST proteins in *A. thaliana* do not have predicted
489 signal peptides for secretion (SignalP-5.0) and are mainly localized in the intracellular
490 compartments (Dixon et al., 2009; Noctor et al., 2012; Lallement et al., 2014). Given
491 that we observed the influence of non-pathogenic inoculations on genes related to
492 cellular redox at relatively late time points (from 4 days to 5 weeks), it is plausible that
493 the cytoplasmic redox regulation is involved in the non-pathogenic interactions, while
494 apoplastic ROS production is involved in the defense response against pathogens.

495 Overall, based on these findings, we speculate that host root intracellular redox status
496 has a role in the discrimination between pathogenic and non-pathogenic interactions,
497 either as a determinant of the response or as a consequence of different types of
498 interactions. Yet, the key molecular signatures in plants and microbes that differentiate
499 pathogenic and non-pathogenic interactions remain to be identified.
500
501 *Rhizobiales commensals interfere with host sulfated peptide pathway to promote root*
502 *growth*
503 We here provide a clear genetic evidence for the role of plant sulfated peptides in
504 Rhizobiales RGP. Plant sulfated peptides characterized thus far mostly play a crucial
505 role in plant development, including cell division, growth, and differentiation
506 (Kaufmann and Sauter, 2019). In roots, RGFs, PSKs, and PSY1 orchestrate with a
507 phytohormonal network to coordinate cell division and growth constitutively as well as
508 in response to environmental conditions (Matsubayashi et al., 2006; Amano et al.,
509 2007; Matsuzaki et al., 2010; Cederholm and Benfey, 2015), while CIFs specifically
510 regulate endodermal cell differentiation (Doblas et al., 2017). Our mutant analysis
511 demonstrated that known receptors of these sulfated peptides were not essential for
512 Rhizobiales RGP. This suggests the presence of unidentified cognate receptors or yet
513 another class of sulfated peptides. Receptors for extracellular peptides are typically a
514 member of the leucine-rich repeat receptor-like kinase (LRR-RLK) superfamily, which
515 has been immensely diversified in land plant lineages (Shiu et al., 2004; Furumizu et
516 al., 2021). To date, only a handful of LRR-RLKs have been functionally characterized,
517 while the physiological function of many members, including their cognate ligands,
518 remain unknown. Of note, while the *pskr1pskr2psy1r* mutant is mostly insensitive to
519 PSKs, it still significantly responds to the PSY1 peptide albeit to a lesser extent than
520 wild-type plants (Pruitt et al., 2017). Given that the direct binding between PSY1 and
521 PSY1R has not yet been experimentally shown, it is sensible to assume the presence
522 of other LRR-RLKs that perceive PSY1 and related peptides (Tost et al., 2021).
523 Besides, a large variety of uncharacterized secreted peptides are encoded by the *A.*
524 *thaliana* genome, including several classes of peptides with a predicted motif for
525 tyrosyl sulfation (aspartate-tyrosin; DY motif; Ghorbani et al., 2015), pointing to an
526 unexplored repertoire of plant sulfated peptides. Further characterization of the
527 mechanisms by which Rhizobiales promote root growth in a manner dependent on the

528 host sulfated peptide pathway may lead to identification of a novel class of receptors
529 and/or ligand sulfated peptides.
530 Interestingly, a hemibiotrophic bacterial pathogen *Xanthomonas oryzae* pv.
531 *oryzae* (*Xoo*) also produces a sulfated peptide, whose amino acid sequence is highly
532 similar to that of plant PSY1. This peptide, called RaxX, is needed for *Xoo* to exert its
533 virulence in rice, which is on the other hand recognized by the host immune receptor
534 XA21 to initiate responses that limit *Xoo* infection (Pruitt et al., 2015; Pruitt et al., 2017).
535 An exogenous treatment of *A. thaliana* plants with RaxX promotes root growth, as
536 does PSY1, and, therefore, it has been speculated that RaxX interferes with the PSY1
537 pathway to interrupt host immunity. Although RaxX has been the only bacterial
538 sulfated peptides that have been molecularly characterized thus far, it is plausible that
539 other bacterial species, especially those interacting with eukaryotic hosts, have
540 acquired the ability to secrete sulfated peptides that mimic and/or interfere with host
541 extracellular peptide signaling. In fact, genes with high similarity to the sulfotransferase
542 RaxST in *Xoo* were found in *A. thaliana* root-associated bacterial genomes (20 out
543 194 genomes, based on blastp with an *E* value cutoff of 1.0; (Bai et al., 2015), mostly
544 in those belonging to the orders Sphingomonadales, Burkholderiales,
545 Pseudomonadales, and Xanthomonadales. It is also possible that, even despite the
546 lack of sequence-related RaxST homologues, other bacterial species have
547 convergently acquired another class of enzymes that catalyze sulfation of secreted
548 peptides. Yet, it is not highly likely that the Rhizobiales RGP is mediated by bacterial
549 sulfated peptides. It is important to note that the TPST enzyme catalyzes tyrosine *O*-
550 sulfation within the Golgi apparatus, most likely at the *cis*-side, before the substrate
551 (pro)peptides reach the apoplast after its translation in the endoplasmic reticulum
552 (Komori et al., 2009). For external peptides to be sulfated by the host TPST, they need
553 to be internalized into the host cells and transported to *cis*-Golgi, followed by tyrosine
554 sulfation by TPST and re-secretion back to the apoplast. Overall, it is probable that
555 the lack of TPST in the host would not directly affect *de novo* production of sulfated
556 peptides by bacterial or mediate sulfation of naïve bacterial peptides in the
557 extracellular space. Our results rather delineate the involvement of plant endogenous
558 sulfated peptides.
559
560
561

562 *Physiological relevance of Rhizobiales RGP*

563 Manipulation of host root growth appears to be a common feature of root-associated
564 commensal bacteria (Zamioudis et al., 2013; Finkel et al., 2020), while one of the most
565 common and dominant pathways is auxin-triggered root growth inhibition (Finkel et al.,
566 2020). Despite the known mechanisms to manipulate host abiotic stress responses
567 via phytohormonal network (Bulgarelli et al., 2013), little is known about the
568 mechanisms by which root commensal promote root growth. Moreover, it is yet to be
569 seen whether root growth phonotypes observed in artificial gnotobiotic system is
570 relevant in the ecological/physiological context. Due to the plasticity and high
571 variability of root growth depending on the environmental conditions, it remains
572 challenging to directly tackle this question using wild-type plants. Here, we provide
573 genetic evidence for the crucial role of sulfated peptides in Rhizobiales RGP. Retained
574 RGP exerted by Pseudomonadales commensals in the *tpst* mutant is indicative of a
575 regulatory role of sulfated peptides, rather than a confounding effect due to a
576 pleiotropic disorganization of the root MZ in this mutant. ANAC060 may also be
577 involved in this interaction, although the evidence remains circumstantial. A genetic
578 analysis of ANAC060 and other related ANAC family TFs is needed to disentangle the
579 transcriptional regulatory machinery that is associated with and possibly responsible
580 for Rhizobiales RGP activity.

581 Our results show that two independent lineages in Alpha- and
582 Gammaproteobacteria classes employ independent mechanisms to promote host root
583 growth, demonstrating that root-associated bacteria have likely acquired RGP
584 capabilities more than once, independently. This, together with the wide prevalence of
585 TPST-dependent RGP in extant Rhizobiales commensals, implies a benefit for
586 bacteria in promoting host root growth, which has given positive selection on this trait.
587 Whether this bacterial pathway actively aims to manipulate host growth or is passively
588 utilized by host to alter their root growth remains to be addressed. A growing collection
589 of microbial strains from a wide range of plant species, including those from an aquatic
590 alga *Chlamydomonas reinhardtii* (Durán et al., 2021), provides a useful tool to address
591 this question. Moreover, identification of bacterial genes responsible for RGP
592 phenotype is of crucial importance to genetically test the impact of this trait on plant
593 and host fitness. We here provide the basis to better understand the molecular dialog
594 between *A. thaliana* roots and Rhizobiales commensals to genetically address the
595 relevance of microbiota-influenced regulation of plant growth and development.

596 **Methods**

597 *Plant materials and growth conditions*

598 We used *A. thaliana* wild-type accession Col-0 (CS60000) and commensal bacterial
599 strains isolated from *A. thaliana* grown in natural soils, as described previously (Bai et
600 al., 2015; Garrido-Oter et al., 2018). Plants were grown under short-day conditions (10
601 h under light at 21°C and 14 h under dark at 19°C) in a square plate (120x120 mm^2)
602 placed vertically within a climate-controlled light cabinet (MLR-352, PHCbi).

603 *Bacterial culture*

604 We used TY media (5 g/L tryptone, 3 g/L yeast extract, 10 mM $CaCl_2$) to grow R129_E,
605 R13_A, Root491, and Root142, and half strength of Tryptic Soy Broth media (15 g/L
606 TSB; Sigma-Aldrich) to grow Root1497 and Root700. Bacterial cells were stored in
607 glycerol stocks (16% v/v) at -80°C and recovered on TY supplemented with 1.8% agar,
608 or 50% TSB supplemented with 1.5% agar, and cultivated at 28°C under dark
609 conditions.

610 *Inoculation of plants with bacteria, root length quantification, and bacterial abundance*
611 *quantification*

612 Inoculation of plants with Alphaproteobacteria was performed as described previously
613 (Garrido-Oter et al., 2018). Briefly, we cultivated bacteria in liquid TY or 50% TSB
614 media for 2 days at 28°C with 180 rpm agitation and mixed bacterial cells into half-
615 strength of Murashige and Skoog media (750 mM $MgSO_4$, 625 mM KH_2PO_4, 10.3 mM
616 NH_4NO_3, 9.4 mM KNO_3, 1.5 mM $CaCl_2$, 55 nM $CoCl_2$, 53 nM $CuCl_2$, 50 mM H_3BO_3,
617 2.5 mM KI, 50 mM $MnCl_2$, 520 nM Na_2MoO_4, 15 mM $ZnCl_2$, 75 mM Fe-EDTA, 500 mM
618 MES-KOH pH 5.5) supplemented with 1% Bacto Agar (Difco). Bacterial titer (OD_{600})
619 was adjusted to 0.00005 by mixing 5 µl of bacterial suspension (OD_{600} = 0.5 in 10 mM
620 $MgCl_2$) into 50 ml of MS media pre-cooled to around 40-50°C. *A. thaliana* seeds were
621 directly placed onto bacterium-containing media or precultured on half-strength of
622 Murashige and Skoog media with vitamin (Duchefa) supplemented with 1% Bacto
623 Agar for 1 week and before seedlings were transferred to the bacterium-containing
624 plates. The same media was supplemented with 1 µM flg22
625 (QRLSTGSRINSAKDDAAGLQIA; EZBiolab), 100 nM RGF1 [D-Y(SO_3H)-SNPGHHP-
626 Hyp-RHN; Beijing Scilight Biotechnology], or dRGF1 [DYSNPGHHP-Hyp-RHN] when
627 necessary. Plates were then recorded by a scanner for root growth quantification using
628 Fiji (Schindelin et al., 2012). Obtained data were square root transformed and fitted to

629 a linear mixed model using biological and technical replicates as random factors, using
630 the lmer function of the *lme4* R package. Fitted data was diagnosed to ensure the
631 normal distribution of residuals and used for Student's *t* test followed by correction for
632 multiple comparison based on the Benjamini-Hochberg method. For bacterial biomass
633 quantification, roots were thoroughly washed twice in sterile water to avoid residual
634 agar pieces and frozen in a 2 ml screw-cap tubes with 1-mm zirconia beads in liquid
635 nitrogen. Quantitative PCR was performed using the genomic DNA extracted from
636 roots by DNeasy Plant Mini Kit (QIAGEN) and primer sets specific to *16S* rRNA gene
637 sequences of *A. thaliana* (5'-CAGGCGGTGGAAACTACCAAG-3' and 5'-
638 TACAGCACTGCACGGGTCGAT-3') and R129_E (5'-
639 CGAGCTAATCTCCAAAAGCCATC-3' and 5'-TGACCCTACCGTGGTTAGCTG-3')
640 with iQ SYBR Green Supermix (BIO-RAD), as described previously (Garrido-Oter et
641 al., 2018).
642 *RNA extraction and sequencing*
643 For transcriptomic analysis of roots inoculated with Alphaproteobacteria commensals,
644 roots inoculated with bacteria for 12 days, as described above, were harvested and
645 immediately frozen in liquid nitrogen. Roots from three plates (approximately 25
646 plants) were pooled into one sample. Three full-factorial biological replicates from
647 three fully independent experiments were prepared for each condition. Roots were
648 then homogenized with 1-mm zirconia beads (Carl Roth) and Precellys24 (6,300 rpm
649 for 30 sec, 2 times with 15-sec intervals; Bertin), and RNA was extracted and purified
650 with the RNeasy Plant Mini kit (QIAGEN). Quality control, library preparation, and
651 sequencing (on the Illumina HiSeq 3000 platform) were conducted at the Max Planck
652 Genome Centre (MPGC), Cologne. Approximately 20,000,000 reads (150-bp single-
653 end) were obtained per sample.
654 For transcriptomic analysis of roots inoculated with R129_E in the presence of flg22,
655 plants were inoculated as described above. Plants from one plate were pooled into
656 one sample (approximately 10 plants) and three independent samples were obtained
657 per condition. Two fully independent experiments were conducted and six samples
658 per condition were obtained. Quality control, library preparation, and sequencing (on
659 the Illumina HiSeq 3000 platform) were conducted at the Max Planck Genome Centre
660 (MPGC), Cologne. Approximately 6,000,000 reads (150-bp single-end) were obtained
661 per sample.

662 For transcriptomic analysis of roots inoculated with *B. phytofirmans* and *B. glumae*,
663 Col-0 plants were grown on vertical agarose plates with Long Ashton nutrient solution
664 adjusted for sulfate concentration of 750 μM (control) or 25 μM (low S) as described
665 before (Koprivova et al., 2019). Total RNA was isolated from 18-day-old (14 dpi) roots
666 and sequenced at the Genomics & Transcriptomics Laboratory (GTL) at Heinrich
667 Heine University, Düsseldorf. Approximately 40,000,000 reads (150-bp single-end)
668 were obtained per sample.
669 *RNA-seq analysis*
670 Obtained reads, as well as reads downloaded from the Sequence Read Archive (SRA)
671 database, were preprocessed by fastp (Chen et al., 2018) with default parameters and
672 aligned to *A. thaliana* Col-0 genome by HISAT2 (Kim et al., 2019) with default
673 parameters based on the latest gene annotation (Cheng et al., 2017). Reads per gene
674 were counted by featureCounts (Liao et al., 2014) with default parameters.
675 Subsequent statistical analyses were performed using R software (https://www.r-
676 project.org/) unless described otherwise. Differential expression analysis was
677 performed using the *edgeR* (Robinson et al., 2010) package. Library size was
678 normalized by the weighted trimmed mean of M-values (TMM) method, and
679 normalized read counts were fitted to a generalized linear model (GLM) with a negative
680 binomial distribution to identify significantly differentially expressed genes (DEGs).
681 Zero-centered expression values were calculated based on $\log_2$ counts per million
682 (log2cpm) by subtracting the mean for each gene across samples. For comparison
683 between datasets, TMM normalization, GLM fitting, and zero-centered expression
684 values were calculated within each dataset. Zero-centered expression values were
685 used to compute *k*-means clustering, where *k* was decided based on Bayesian
686 Information Criterion (BIC). The similarity between samples was inferred by computing
687 Pearson's Correlation Coefficients (PCC) based on zero-centered expression values
688 of DEGs (n = 1,439). Distance of PCCs to 1 was used as dissimilarity indices to
689 perform principal coordinates analysis (PCoA) by cmdscale function. GO enrichment
690 analysis was performed by Metascape online software (Zhou et al., 2019).
691 Transcription binding motif enrichment analysis was performed using the ame function
692 implemented in the MEME Suite (McLeay and Bailey, 2010). Gene regulatory network
693 inference was performed using the *GENIE3* package (Huynh-Thu et al., 2010) with
694 default parameters. We compared responses to different microbes by computing
695 logFC within each dataset and use it to compute cosine similarity by the cosine

696 function in the packge *lsa* and performed *k*-means clustering, whose *k* was determined
697 based on the Bayesian Information Criterion. Distance of cosine similarities to 1 was
698 used as dissimilarity indices to perform PCoA and CAP. Permutational analysis of
699 variance (PERMANOVA) and pairwise PERMANOVA were performed by the adonis2
700 and pairwise.perm.manova functions of the packages *vegan* and *RVAideMemoire*
701 packages. All plots were visualized by Metascape or by the *ggplot2*, *ggtree*, *patchwork*,
702 and *igraph* packages in R.

703 *Single-cell RNA-seq analysis*

704 T-distributed Stochastic Neighbor Embedding (t-SNE) and representation of cluster-
705 wise expression levels as a violin plot were created by The Plant Single Cell RNA-
706 Sequencing Database (https://www.zmbp-resources.uni-
707 tuebingen.de/timmermans/plant-single-cell-browser/). To perform co-expression
708 analysis, read count data of 27,629 genes from 4,727 cells was retrieved from the
709 NCBI Sequence Read Archive (SRA) under the accession number GSE123818,
710 followed by global-scaling normalization by the NormalizeData function in the *Seurat*
711 package (Hao et al., 2020). We then filtered for 22,017 highly variable genes and their
712 expression values were scaled and centered by the FindVariableGenes and
713 ScaleData functions. Normalized and scaled expression values were used to compute
714 mutual ranks as a co-expression index for all pairs of genes as described previously
715 (Obayashi and Kinoshita, 2009). The top 100 genes co-expressed with *ANAC060*
716 were selected based on the mutual ranks and their GO enrichment was analyzed by
717 Metascape.

718 *Confocal microscopy*

719 Root tips (1-2 cm) were excised on agar plates and mounted onto a slide glass with
720 Milli-Q water or 10 μg/ml propidium iodide (PI). PI and GFP fluorescence were
721 observed by a SP8 FALCON-DIVE confocal microscope (Leica) using the 2-photon
722 excitation at XXX nm for GFP and 1,045 nm for PI excitation and emission at XXX-
723 XXX for GFP and XXX-XXX nm for PI, or by a LSM780 confocal microscope (Zeiss)
724 using the 488-nm line of a 25-mW Argon ion laser for GFP.

725 For EdU staining, roots of seed-inoculated plants at 21 dpi were incubated with
726 EdU for two hours directly on agar plates, followed by fixation with 2% formaldehyde,
727 0.3% glutaraldehyde, 0.1% Triton X-100, 10 mM EGTA, and 5 mM $MgSO_4$ in 50 mM
728 sodium phosphate buffer (pH 7.2) for 1 hour, washing with phospho-buffered saline,

729 and staining with Alexa488-azide using the Click-iT EdU Cell Proliferation Kit (Thermo
730 Fisher). Stained roots were observed under a LSM780 confocal microscope (Zeiss)
731 using the 488-nm line of a 25-mW Argon ion laser.
732 All acquired images were processed and adjusted (equally within each
733 experiment) by Fiji (Schindelin et al., 2012).
734 *Data and code availability*
735 Raw sequencing reads obtained in this study are deposited to the European
736 Nucleotide Archive (ENA) under the accession numbers of PRJEB45043
737 (Alphaproteobacteria), PRJEB45044 (R129_E with flg22), and PRJEB45045
738 (*Burkholderia*). The scripts for the computational analyses described in this study are
739 available at https://github.com/rtnakano1984/RNAseq_Alphaproteobacteria and
740 https://github.com/rtnakano1984/RNAseq_compare to ensure replicability and
741 reproducibility of these results.
742
743 **Acknowledgments**
744 We would like to thank Paul Schulze-Lefert at the Max Planck Institute for Plant
745 Breeding Research for providing infrastructures and helpful advice for this study, Jiri
746 Friml at the Institute of Science and Technology Austria, Niko Geldner at the University
747 of Lausanne, Woei-Jiun Guo at the National Cheng Kung University, Yoshikatsu
748 Matsubayashi and Hidefumi Shinohara at the Nagoya University, Birgit Kemmerling at
749 the University of Tübingen, Jia Li at the Lanzhou University, Margret Sauter at the
750 University of Kiel, and Bruno Müller at the University of Zurich for providing *A. thaliana*
751 mutant and transgenic seeds, Bruno Hüttel and Mark Holstein at the MPGC and
752 Patrick Petzsch and Karl-Erich Köhler at the GTL for sequencing, and Christina Phillip
753 and Petra Köchner for their technical support. We also would like to thank Tatsuya
754 Nobori, Kenichi Tsuda, Stephane Hacquard, and Rozina Kardakaris for their critical
755 reading and help editing the manuscript. This work was supported by the Deutsche
756 Forschungsgemeinschaft (DFG, German Research Foundation) under the Priority
757 Programme "2125 Deconstruction and Reconstruction of Plant Microbiota
758 (DECRyPT)" funded to RTN (402201269) and SK (401836049). This work was also
759 supported by the Cluster of Excellence on Plant Sciences (CEPLAS) funded by DFG
760 to TG, SK and GWK. The authors declare no conflicts of interest. In memory of Alina
761 Kuroczik, who provided technical support for this study.
762

763 **Author contribution**

764 RTN designed the research and performed experiments. JH, TG, and AK performed
765 experiments partly under supervision of RTN and SK. PS, MNC and GWK contributed
766 to the RNAseq data analysis. RTN analyzed and interpreted the data. RTN wrote the
767 paper with inputs from the other authors.

768

769 **References**

770 **Achard, P., Gusti, A., Cheminant, S., Alioua, M., Dhondt, S., Coppens, F.,**
771 **Beemster, G.T., and Genschik, P.** (2009). Gibberellin signaling controls cell
772 proliferation rate in Arabidopsis. Curr Biol **19,** 1188-1193.
773 **Aida, M., Beis, D., Heidstra, R., Willemsen, V., Blilou, I., Galinha, C., Nussaume,**
774 **L., Noh, Y.S., Amasino, R., and Scheres, B.** (2004). The PLETHORA genes
775 mediate patterning of the Arabidopsis root stem cell niche. Cell **119,** 109-120.
776 **Amano, Y., Tsubouchi, H., Shinohara, H., Ogawa, M., and Matsubayashi, Y.**
777 (2007). Tyrosine-sulfated glycopeptide involved in cellular proliferation and
778 expansion in Arabidopsis. Proc Natl Acad Sci U S A **104,** 18333-18338.
779 **Arnaud, D., Deeks, M.J., and Smirnoff, N.** (2021). Differences between apoplastic
780 and cytosolic reactive oxygen species production in Arabidopsis during pattern-
781 triggered immunity. bioRxiv, 2021.2004.2020.440614.
782 **Bai, Y., Muller, D.B., Srinivas, G., Garrido-Oter, R., Potthoff, E., Rott, M.,**
783 **Dombrowski, N., Munch, P.C., Spaepen, S., Remus-Emsermann, M., Huttel,**
784 **B., McHardy, A.C., Vorholt, J.A., and Schulze-Lefert, P.** (2015). Functional
785 overlap of the Arabidopsis leaf and root microbiota. Nature **528,** 364-369.
786 **Berg, G., Rybakova, D., Fischer, D., Cernava, T., Verges, M.C., Charles, T., Chen,**
787 **X., Cocolin, L., Eversole, K., Corral, G.H., Kazou, M., Kinkel, L., Lange, L.,**
788 **Lima, N., Loy, A., Macklin, J.A., Maguin, E., Mauchline, T., McClure, R.,**
789 **Mitter, B., Ryan, M., Sarand, I., Smidt, H., Schelkle, B., Roume, H., Kiran,**
790 **G.S., Selvin, J., Souza, R.S.C., van Overbeek, L., Singh, B.K., Wagner, M.,**
791 **Walsh, A., Sessitsch, A., and Schloter, M.** (2020). Microbiome definition re-
792 visited: old concepts and new challenges. Microbiome **8,** 103.
793 **Bulgarelli, D., Schlaeppi, K., Spaepen, S., Ver Loren van Themaat, E., and**
794 **Schulze-Lefert, P.** (2013). Structure and functions of the bacterial microbiota
795 of plants. Annu Rev Plant Biol **64,** 807-838.
796 **Bulgarelli, D., Rott, M., Schlaeppi, K., Ver Loren van Themaat, E., Ahmadinejad,**
797 **N., Assenza, F., Rauf, P., Huettel, B., Reinhardt, R., Schmelzer, E., Peplies,**
798 **J., Gloeckner, F.O., Amann, R., Eickhorst, T., and Schulze-Lefert, P.** (2012).
799 Revealing structure and assembly cues for Arabidopsis root-inhabiting bacterial
800 microbiota. Nature **488,** 91-95.
801 **Castrillo, G., Teixeira, P.J., Paredes, S.H., Law, T.F., de Lorenzo, L., Feltcher,**
802 **M.E., Finkel, O.M., Breakfield, N.W., Mieczkowski, P., Jones, C.D., Paz-**
803 **Ares, J., and Dangl, J.L.** (2017). Root microbiota drive direct integration of
804 phosphate stress and immunity. Nature **543,** 513-518.
805 **Cederholm, H.M., and Benfey, P.N.** (2015). Distinct sensitivities to phosphate
806 deprivation suggest that RGF peptides play disparate roles in Arabidopsis
807 thaliana root development. New Phytol **207,** 683-691.

808 **Chaiwanon, J., and Wang, Z.Y.** (2015). Spatiotemporal brassinosteroid signaling and
809 antagonism with auxin pattern stem cell dynamics in Arabidopsis roots. Curr
810 Biol **25,** 1031-1042.
811 **Chen, S., Zhou, Y., Chen, Y., and Gu, J.** (2018). fastp: an ultra-fast all-in-one FASTQ
812 preprocessor. Bioinformatics **34,** i884-i890.
813 **Chen, T., Nomura, K., Wang, X., Sohrabi, R., Xu, J., Yao, L., Paasch, B.C., Ma, L.,**
814 **Kremer, J., Cheng, Y., Zhang, L., Wang, N., Wang, E., Xin, X.F., and He,**
815 **S.Y.** (2020). A plant genetic network for preventing dysbiosis in the
816 phyllosphere. Nature **580,** 653-657.
817 **Cheng, C.Y., Krishnakumar, V., Chan, A.P., Thibaud-Nissen, F., Schobel, S., and**
818 **Town, C.D.** (2017). Araport11: a complete reannotation of the Arabidopsis
819 thaliana reference genome. Plant J **89,** 789-804.
820 **Dello Ioio, R., Nakamura, K., Moubayidin, L., Perilli, S., Taniguchi, M., Morita,**
821 **M.T., Aoyama, T., Costantino, P., and Sabatini, S.** (2008). A genetic
822 framework for the control of cell division and differentiation in the root meristem.
823 Science **322,** 1380-1384.
824 **Denyer, T., Ma, X., Klesen, S., Scacchi, E., Nieselt, K., and Timmermans, M.C.P.**
825 (2019). Spatiotemporal Developmental Trajectories in the Arabidopsis Root
826 Revealed Using High-Throughput Single-Cell RNA Sequencing. Dev Cell **48,**
827 840-852 e845.
828 **Di Mambro, R., De Ruvo, M., Pacifici, E., Salvi, E., Sozzani, R., Benfey, P.N.,**
829 **Busch, W., Novak, O., Ljung, K., Di Paola, L., Maree, A.F.M., Costantino,**
830 **P., Grieneisen, V.A., and Sabatini, S.** (2017). Auxin minimum triggers the
831 developmental switch from cell division to cell differentiation in the Arabidopsis
832 root. Proc Natl Acad Sci U S A **114,** E7641-E7649.
833 **Dixon, D.P., Skipsey, M., and Edwards, R.** (2010). Roles for glutathione transferases
834 in plant secondary metabolism. Phytochemistry **71,** 338-350.
835 **Dixon, D.P., Hawkins, T., Hussey, P.J., and Edwards, R.** (2009). Enzyme activities
836 and subcellular localization of members of the Arabidopsis glutathione
837 transferase superfamily. J Exp Bot **60,** 1207-1218.
838 **Doblas, V.G., Smakowska-Luzan, E., Fujita, S., Alassimone, J., Barberon, M.,**
839 **Madalinski, M., Belkhadir, Y., and Geldner, N.** (2017). Root diffusion barrier
840 control by a vasculature-derived peptide binding to the SGN3 receptor. Science
841 **355,** 280-284.
842 **Duran, P., Thiergart, T., Garrido-Oter, R., Agler, M., Kemen, E., Schulze-Lefert,**
843 **P., and Hacquard, S.** (2018). Microbial Interkingdom Interactions in Roots
844 Promote Arabidopsis Survival. Cell **175,** 973-983 e914.
845 **Durán, P., Flores-Uribe, J., Wippel, K., Zhang, P., Guan, R., and Garrido-Oter, R.**
846 (2021). Characterization of the Chlamydomonas reinhardtii phycosphere
847 reveals conserved features of the plant microbiota. bioRxiv,
848 2021.2003.2004.433956.
849 **Eulgem, T., and Somssich, I.E.** (2007). Networks of WRKY transcription factors in
850 defense signaling. Curr Opin Plant Biol **10,** 366-371.
851 **Finkel, O.M., Salas-Gonzalez, I., Castrillo, G., Conway, J.M., Law, T.F., Teixeira,**
852 **P., Wilson, E.D., Fitzpatrick, C.R., Jones, C.D., and Dangl, J.L.** (2020). A
853 single bacterial genus maintains root growth in a complex microbiome. Nature
854 **587,** 103-108.
855 **Furumizu, C., Krabberød, A.K., Hammerstad, M., Alling, R.M., Wildhagen, M.,**
856 **Sawa, S., and Aalen, R.B.** (2021). The Sequenced Genomes of Non-Flowering

857 Land Plants Reveal the (R)Evolutionary History of Peptide Signaling. bioRxiv,
858 2020.2006.2002.130120.
859 **Galinha, C., Hofhuis, H., Luijten, M., Willemsen, V., Blilou, I., Heidstra, R., and**
860 **Scheres, B.** (2007). PLETHORA proteins as dose-dependent master
861 regulators of Arabidopsis root development. Nature **449,** 1053-1057.
862 **Garrido-Oter, R., Nakano, R.T., Dombrowski, N., Ma, K.W., AgBiome, T., McHardy,**
863 **A.C., and Schulze-Lefert, P.** (2018). Modular Traits of the Rhizobiales Root
864 Microbiota and Their Evolutionary Relationship with Symbiotic Rhizobia. Cell
865 Host Microbe **24,** 155-167 e155.
866 **Ghorbani, S., Lin, Y.C., Parizot, B., Fernandez, A., Njo, M.F., Van de Peer, Y.,**
867 **Beeckman, T., and Hilson, P.** (2015). Expanding the repertoire of secretory
868 peptides controlling root development with comparative genome analysis and
869 functional assays. J Exp Bot **66,** 5257-5269.
870 **Gomez-Gomez, L., Felix, G., and Boller, T.** (1999). A single locus determines
871 sensitivity to bacterial flagellin in Arabidopsis thaliana. Plant J **18,** 277-284.
872 **Hacquard, S., Garrido-Oter, R., Gonzalez, A., Spaepen, S., Ackermann, G.,**
873 **Lebeis, S., McHardy, A.C., Dangl, J.L., Knight, R., Ley, R., and Schulze-**
874 **Lefert, P.** (2015). Microbiota and Host Nutrition across Plant and Animal
875 Kingdoms. Cell Host Microbe **17,** 603-616.
876 **Hacquard, S., Kracher, B., Hiruma, K., Munch, P.C., Garrido-Oter, R., Thon, M.R.,**
877 **Weimann, A., Damm, U., Dallery, J.F., Hainaut, M., Henrissat, B., Lespinet,**
878 **O., Sacristan, S., Ver Loren van Themaat, E., Kemen, E., McHardy, A.C.,**
879 **Schulze-Lefert, P., and O'Connell, R.J.** (2016). Survival trade-offs in plant
880 roots during colonization by closely related beneficial and pathogenic fungi. Nat
881 Commun **7,** 11362.
882 **Hao, Y., Hao, S., Andersen-Nissen, E., Mauck, W.M., Zheng, S., Butler, A., Lee,**
883 **M.J., Wilk, A.J., Darby, C., Zagar, M., Hoffman, P., Stoeckius, M., Papalexi,**
884 **E., Mimitou, E.P., Jain, J., Srivastava, A., Stuart, T., Fleming, L.B., Yeung,**
885 **B., Rogers, A.J., McElrath, J.M., Blish, C.A., Gottardo, R., Smibert, P., and**
886 **Satija, R.** (2020). Integrated analysis of multimodal single-cell data. bioRxiv,
887 2020.2010.2012.335331.
888 **Harbort, C.J., Hashimoto, M., Inoue, H., Niu, Y., Guan, R., Rombola, A.D., Kopriva,**
889 **S., Voges, M., Sattely, E.S., Garrido-Oter, R., and Schulze-Lefert, P.** (2020).
890 Root-Secreted Coumarins and the Microbiota Interact to Improve Iron Nutrition
891 in Arabidopsis. Cell Host Microbe **28,** 825-837 e826.
892 **Hartmann, M., Zeier, T., Bernsdorff, F., Reichel-Deland, V., Kim, D., Hohmann, M.,**
893 **Scholten, N., Schuck, S., Brautigam, A., Holzel, T., Ganter, C., and Zeier,**
894 **J.** (2018). Flavin Monooxygenase-Generated N-Hydroxypipecolic Acid Is a
895 Critical Element of Plant Systemic Immunity. Cell **173,** 456-469 e416.
896 **Hiruma, K., Gerlach, N., Sacristan, S., Nakano, R.T., Hacquard, S., Kracher, B.,**
897 **Neumann, U., Ramirez, D., Bucher, M., O'Connell, R.J., and Schulze-Lefert,**
898 **P.** (2016). Root Endophyte Colletotrichum tofieldiae Confers Plant Fitness
899 Benefits that Are Phosphate Status Dependent. Cell **165,** 464-474.
900 **Hou, S., Thiergart, T., Vannier, N., Mesny, F., Ziegler, J., Pickel, B., and Hacquard,**
901 **S.** (2020). Microbiota-root-shoot axis modulation by MYC2 favours Arabidopsis
902 growth over defence under suboptimal light. bioRxiv, 2020.2011.2006.371146.
903 **Hsu, F.C., Chou, M.Y., Chou, S.J., Li, Y.R., Peng, H.P., and Shih, M.C.** (2013).
904 Submergence confers immunity mediated by the WRKY22 transcription factor
905 in Arabidopsis. Plant Cell **25,** 2699-2713.

Huffaker, A., and Ryan, C.A. (2007). Endogenous peptide defense signals in Arabidopsis differentially amplify signaling for the innate immune response. Proc Natl Acad Sci U S A **104,** 10732-10736.

Huot, B., Yao, J., Montgomery, B.L., and He, S.Y. (2014). Growth-defense tradeoffs in plants: a balancing act to optimize fitness. Mol Plant **7,** 1267-1287.

Huynh-Thu, V.A., Irrthum, A., Wehenkel, L., and Geurts, P. (2010). Inferring regulatory networks from expression data using tree-based methods. PLoS One **5**.

Kaufmann, C., and Sauter, M. (2019). Sulfated plant peptide hormones. J Exp Bot **70,** 4267-4277.

Kim, D., Paggi, J.M., Park, C., Bennett, C., and Salzberg, S.L. (2019). Graph-based genome alignment and genotyping with HISAT2 and HISAT-genotype. Nat Biotechnol **37,** 907-915.

Kim, H.J., Park, J.H., Kim, J., Kim, J.J., Hong, S., Kim, J., Kim, J.H., Woo, H.R., Hyeon, C., Lim, P.O., Nam, H.G., and Hwang, D. (2018). Time-evolving genetic networks reveal a NAC troika that negatively regulates leaf senescence in Arabidopsis. Proc Natl Acad Sci U S A **115,** E4930-E4939.

Komori, R., Amano, Y., Ogawa-Ohnishi, M., and Matsubayashi, Y. (2009). Identification of tyrosylprotein sulfotransferase in Arabidopsis. Proc Natl Acad Sci U S A **106,** 15067-15072.

Koprivova, A., Schuck, S., Jacoby, R.P., Klinkhammer, I., Welter, B., Leson, L., Martyn, A., Nauen, J., Grabenhorst, N., Mandelkow, J.F., Zuccaro, A., Zeier, J., and Kopriva, S. (2019). Root-specific camalexin biosynthesis controls the plant growth-promoting effects of multiple bacterial strains. Proc Natl Acad Sci U S A **116,** 15735-15744.

Ladwig, F., Dahlke, R.I., Stuhrwohldt, N., Hartmann, J., Harter, K., and Sauter, M. (2015). Phytosulfokine Regulates Growth in Arabidopsis through a Response Module at the Plasma Membrane That Includes CYCLIC NUCLEOTIDE-GATED CHANNEL17, H+-ATPase, and BAK1. Plant Cell **27,** 1718-1729.

Lallement, P.A., Brouwer, B., Keech, O., Hecker, A., and Rouhier, N. (2014). The still mysterious roles of cysteine-containing glutathione transferases in plants. Front Pharmacol **5,** 192.

Liao, Y., Smyth, G.K., and Shi, W. (2014). featureCounts: an efficient general purpose program for assigning sequence reads to genomic features. Bioinformatics **30,** 923-930.

Lu, X., Shi, H., Ou, Y., Cui, Y., Chang, J., Peng, L., Gou, X., He, K., and Li, J. (2020). RGF1-RGI1, a Peptide-Receptor Complex, Regulates Arabidopsis Root Meristem Development via a MAPK Signaling Cascade. Mol Plant **13,** 1594-1607.

Lundberg, D., Persson, I., and Ekberg, C. (2013). Crystal structure of [Eu(CyMe4-BTBP)2kappa2O,O'-(NO3)](NO3)2.n-C8H17OH and its structure in 1-octanol solution. Dalton Trans **42,** 3767-3770.

Ma, K.-W., Niu, Y., Jia, Y., Ordon, J., Copeland, C., Emonet, A., Geldner, N., Guan, R., Stolze, S.C., Nakagami, H., Garrido-Oter, R., and Schulze-Lefert, P. (2021). Coordination of microbe–host homeostasis by crosstalk with plant innate immunity. Nature Plants.

Maier, B.A., Kiefer, P., Field, C.M., Hemmerle, L., Bortfeld-Miller, M., Emmenegger, B., Schafer, M., Pfeilmeier, S., Sunagawa, S., Vogel, C.M., and Vorholt, J.A. (2021). A general non-self response as part of plant immunity. Nat Plants **7,** 696-705.

Matsubayashi, Y., Ogawa, M., Kihara, H., Niwa, M., and Sakagami, Y. (2006). Disruption and overexpression of Arabidopsis phytosulfokine receptor gene affects cellular longevity and potential for growth. Plant Physiol **142,** 45-53.

Matsuzaki, Y., Ogawa-Ohnishi, M., Mori, A., and Matsubayashi, Y. (2010). Secreted peptide signals required for maintenance of root stem cell niche in Arabidopsis. Science **329,** 1065-1067.

McLeay, R.C., and Bailey, T.L. (2010). Motif Enrichment Analysis: a unified framework and an evaluation on ChIP data. BMC Bioinformatics **11,** 165.

Nobori, T., Cao, Y., Entila, F., Dahms, E., Tsuda, Y., Garrido-Oter, R., and Tsuda, K. (2021). Dissecting the co-transcriptome landscape of plants and microbiota members. bioRxiv, 2021.2004.2025.440543.

Noctor, G., Mhamdi, A., Chaouch, S., Han, Y., Neukermans, J., Marquez-Garcia, B., Queval, G., and Foyer, C.H. (2012). Glutathione in plants: an integrated overview. Plant Cell Environ **35,** 454-484.

Obayashi, T., and Kinoshita, K. (2009). Rank of correlation coefficient as a comparable measure for biological significance of gene coexpression. DNA Res **16,** 249-260.

Ou, Y., Lu, X., Zi, Q., Xun, Q., Zhang, J., Wu, Y., Shi, H., Wei, Z., Zhao, B., Zhang, X., He, K., Gou, X., Li, C., and Li, J. (2016). RGF1 INSENSITIVE 1 to 5, a group of LRR receptor-like kinases, are essential for the perception of root meristem growth factor 1 in Arabidopsis thaliana. Cell Res **26,** 686-698.

Paasch, B.C., and He, S.Y. (2021). Toward understanding microbiota homeostasis in the plant kingdom. PLoS Pathog **17,** e1009472.

Phukan, U.J., Jeena, G.S., and Shukla, R.K. (2016). WRKY Transcription Factors: Molecular Regulation and Stress Responses in Plants. Front Plant Sci **7,** 760.

Pislewska-Bednarek, M., Nakano, R.T., Hiruma, K., Pastorczyk, M., Sanchez-Vallet, A., Singkaravanit-Ogawa, S., Ciesiolka, D., Takano, Y., Molina, A., Schulze-Lefert, P., and Bednarek, P. (2018). Glutathione Transferase U13 Functions in Pathogen-Triggered Glucosinolate Metabolism. Plant Physiol **176,** 538-551.

Pruitt, R.N., Joe, A., Zhang, W., Feng, W., Stewart, V., Schwessinger, B., Dinneny, J.R., and Ronald, P.C. (2017). A microbially derived tyrosine-sulfated peptide mimics a plant peptide hormone. New Phytol **215,** 725-736.

Pruitt, R.N., Schwessinger, B., Joe, A., Thomas, N., Liu, F., Albert, M., Robinson, M.R., Chan, L.J., Luu, D.D., Chen, H., Bahar, O., Daudi, A., De Vleesschauwer, D., Caddell, D., Zhang, W., Zhao, X., Li, X., Heazlewood, J.L., Ruan, D., Majumder, D., Chern, M., Kalbacher, H., Midha, S., Patil, P.B., Sonti, R.V., Petzold, C.J., Liu, C.C., Brodbelt, J.S., Felix, G., and Ronald, P.C. (2015). The rice immune receptor XA21 recognizes a tyrosine-sulfated protein from a Gram-negative bacterium. Sci Adv **1,** e1500245.

Pucciariello, C., Parlanti, S., Banti, V., Novi, G., and Perata, P. (2012). Reactive oxygen species-driven transcription in Arabidopsis under oxygen deprivation. Plant Physiol **159,** 184-196.

Rajniak, J., Barco, B., Clay, N.K., and Sattely, E.S. (2015). A new cyanogenic metabolite in Arabidopsis required for inducible pathogen defence. Nature **525,** 376-379.

Rasul, S., Dubreuil-Maurizi, C., Lamotte, O., Koen, E., Poinssot, B., Alcaraz, G., Wendehenne, D., and Jeandroz, S. (2012). Nitric oxide production mediates oligogalacturonide-triggered immunity and resistance to Botrytis cinerea in Arabidopsis thaliana. Plant Cell Environ **35,** 1483-1499.

1006 **Rich-Griffin, C., Eichmann, R., Reitz, M.U., Hermann, S., Woolley-Allen, K.,**
1007 **Brown, P.E., Wiwatdirekkul, K., Esteban, E., Pasha, A., Kogel, K.H.,**
1008 **Provart, N.J., Ott, S., and Schafer, P.** (2020). Regulation of Cell Type-Specific
1009 Immunity Networks in Arabidopsis Roots. Plant Cell **32,** 2742-2762.
1010 **Robinson, M.D., McCarthy, D.J., and Smyth, G.K.** (2010). edgeR: a Bioconductor
1011 package for differential expression analysis of digital gene expression data.
1012 Bioinformatics **26,** 139-140.
1013 **Salas-Gonzalez, I., Reyt, G., Flis, P., Custodio, V., Gopaulchan, D., Bakhoum, N.,**
1014 **Dew, T.P., Suresh, K., Franke, R.B., Dangl, J.L., Salt, D.E., and Castrillo, G.**
1015 (2021). Coordination between microbiota and root endodermis supports plant
1016 mineral nutrient homeostasis. Science **371,** eabd0695.
1017 **Schindelin, J., Arganda-Carreras, I., Frise, E., Kaynig, V., Longair, M., Pietzsch,**
1018 **T., Preibisch, S., Rueden, C., Saalfeld, S., Schmid, B., Tinevez, J.Y., White,**
1019 **D.J., Hartenstein, V., Eliceiri, K., Tomancak, P., and Cardona, A.** (2012).
1020 Fiji: an open-source platform for biological-image analysis. Nat Methods **9,** 676-
1021 682.
1022 **Shao, H., Wang, H., and Tang, X.** (2015). NAC transcription factors in plant multiple
1023 abiotic stress responses: progress and prospects. Front Plant Sci **6,** 902.
1024 **Shao, Y., Yu, X., Xu, X., Li, Y., Yuan, W., Xu, Y., Mao, C., Zhang, S., and Xu, J.**
1025 (2020). The YDA-MKK4/MKK5-MPK3/MPK6 Cascade Functions Downstream
1026 of the RGF1-RGI Ligand-Receptor Pair in Regulating Mitotic Activity in Root
1027 Apical Meristem. Mol Plant **13,** 1608-1623.
1028 **Shinohara, H.** (2021). Root meristem growth factor RGF, a sulfated peptide hormone
1029 in plants. Peptides **142,** 170556.
1030 **Shiu, S.H., Karlowski, W.M., Pan, R., Tzeng, Y.H., Mayer, K.F., and Li, W.H.** (2004).
1031 Comparative analysis of the receptor-like kinase family in Arabidopsis and rice.
1032 Plant Cell **16,** 1220-1234.
1033 **Song, W., Liu, L., Wang, J., Wu, Z., Zhang, H., Tang, J., Lin, G., Wang, Y., Wen,**
1034 **X., Li, W., Han, Z., Guo, H., and Chai, J.** (2016). Signature motif-guided
1035 identification of receptors for peptide hormones essential for root meristem
1036 growth. Cell Res **26,** 674-685.
1037 **Teixeira, P., Colaianni, N.R., Law, T.F., Conway, J.M., Gilbert, S., Li, H., Salas-**
1038 **Gonzalez, I., Panda, D., Del Risco, N.M., Finkel, O.M., Castrillo, G.,**
1039 **Mieczkowski, P., Jones, C.D., and Dangl, J.L.** (2021). Specific modulation of
1040 the root immune system by a community of commensal bacteria. Proc Natl
1041 Acad Sci U S A **118,** e2100678118.
1042 **Thiergart, T., Duran, P., Ellis, T., Vannier, N., Garrido-Oter, R., Kemen, E., Roux,**
1043 **F., Alonso-Blanco, C., Agren, J., Schulze-Lefert, P., and Hacquard, S.**
1044 (2020). Root microbiota assembly and adaptive differentiation among
1045 European Arabidopsis populations. Nat Ecol Evol **4,** 122-131.
1046 **Tost, A.S., Kristensen, A., Olsen, L.I., Axelsen, K.B., and Fuglsang, A.T.** (2021).
1047 The PSY Peptide Family-Expression, Modification and Physiological
1048 Implications. Genes (Basel) **12**.
1049 **Tsukagoshi, H., Busch, W., and Benfey, P.N.** (2010). Transcriptional regulation of
1050 ROS controls transition from proliferation to differentiation in the root. Cell **143,**
1051 606-616.
1052 **Ubeda-Tomas, S., Federici, F., Casimiro, I., Beemster, G.T., Bhalerao, R., Swarup,**
1053 **R., Doerner, P., Haseloff, J., and Bennett, M.J.** (2009). Gibberellin signaling
1054 in the endodermis controls Arabidopsis root meristem size. Curr Biol **19,** 1194-
1055 1199.

1056 **Wagner, M.R., Lundberg, D.S., Del Rio, T.G., Tringe, S.G., Dangl, J.L., and**
1057 **Mitchell-Olds, T.** (2016). Host genotype and age shape the leaf and root
1058 microbiomes of a wild perennial plant. Nat Commun **7,** 12151.
1059 **Wang, L., Tsuda, K., Sato, M., Cohen, J.D., Katagiri, F., and Glazebrook, J.** (2009).
1060 Arabidopsis CaM binding protein CBP60g contributes to MAMP-induced SA
1061 accumulation and is involved in disease resistance against Pseudomonas
1062 syringae. PLoS Pathog **5,** e1000301.
1063 **Wang, S., Meade, A., Lam, H.M., and Luo, H.** (2020). Evolutionary Timeline and
1064 Genomic Plasticity Underlying the Lifestyle Diversity in Rhizobiales. mSystems
1065 **5,** e00438-00420.
1066 **Wei, Z., Yang, T., Friman, V.P., Xu, Y., Shen, Q., and Jousset, A.** (2015). Trophic
1067 network architecture of root-associated bacterial communities determines
1068 pathogen invasion and plant health. Nat Commun **6,** 8413.
1069 **Wippel, K., Tao, K., Niu, Y., Zgadzaj, R., Guan, R., Dahms, E., Zhang, P., Jensen,**
1070 **D.B., Logemann, E., Radutoiu, S., Schulze-Lefert, P., and Garrido-Oter, R.**
1071 (2021). Host preference and invasiveness of commensals in the Lotus and
1072 Arabidopsis root microbiota. bioRxiv**,** 2021.2001.2012.426357.
1073 **Yamada, M., Han, X., and Benfey, P.N.** (2020). RGF1 controls root meristem size
1074 through ROS signalling. Nature **577,** 85-88.
1075 **Yu, B., Wang, Y., Zhou, H., Li, P., Liu, C., Chen, S., Peng, Y., Zhang, Y., and Teng,**
1076 **S.** (2020). Genome-wide binding analysis reveals that ANAC060 directly
1077 represses sugar-induced transcription of ABI5 in Arabidopsis. Plant J **103,** 965-
1078 979.
1079 **Yu, K., Liu, Y., Tichelaar, R., Savant, N., Lagendijk, E., van Kuijk, S.J.L., Stringlis,**
1080 **I.A., van Dijken, A.J.H., Pieterse, C.M.J., Bakker, P., Haney, C.H., and**
1081 **Berendsen, R.L.** (2019). Rhizosphere-Associated Pseudomonas Suppress
1082 Local Root Immune Responses by Gluconic Acid-Mediated Lowering of
1083 Environmental pH. Curr Biol **29,** 3913-3920 e3914.
1084 **Yu, P., He, X., Baer, M., Beirinckx, S., Tian, T., Moya, Y.A.T., Zhang, X.,**
1085 **Deichmann, M., Frey, F.P., Bresgen, V., Li, C., Razavi, B.S., Schaaf, G., von**
1086 **Wiren, N., Su, Z., Bucher, M., Tsuda, K., Goormachtig, S., Chen, X., and**
1087 **Hochholdinger, F.** (2021). Plant flavones enrich rhizosphere
1088 Oxalobacteraceae to improve maize performance under nitrogen deprivation.
1089 Nat Plants **7,** 481-499.
1090 **Yuan, X., Wang, H., Cai, J., Li, D., and Song, F.** (2019). NAC transcription factors in
1091 plant immunity. Phytopathology Research **1,** 3.
1092 **Zamioudis, C., Mastranesti, P., Dhonukshe, P., Blilou, I., and Pieterse, C.M.**
1093 (2013). Unraveling root developmental programs initiated by beneficial
1094 Pseudomonas spp. bacteria. Plant Physiol **162,** 304-318.
1095 **Zgadzaj, R., Garrido-Oter, R., Jensen, D.B., Koprivova, A., Schulze-Lefert, P., and**
1096 **Radutoiu, S.** (2016). Root nodule symbiosis in Lotus japonicus drives the
1097 establishment of distinctive rhizosphere, root, and nodule bacterial
1098 communities. Proc Natl Acad Sci U S A **113,** E7996-E8005.
1099 **Zhou, W., Wei, L., Xu, J., Zhai, Q., Jiang, H., Chen, R., Chen, Q., Sun, J., Chu, J.,**
1100 **Zhu, L., Liu, C.M., and Li, C.** (2010). Arabidopsis Tyrosylprotein
1101 sulfotransferase acts in the auxin/PLETHORA pathway in regulating
1102 postembryonic maintenance of the root stem cell niche. Plant Cell **22,** 3692-
1103 3709.

Zhou, Y., Zhou, B., Pache, L., Chang, M., Khodabakhshi, A.H., Tanaseichuk, O., Benner, C., and Chanda, S.K. (2019). Metascape provides a biologist-oriented resource for the analysis of systems-level datasets. Nat Commun **10,** 1523.

Tables

Figure and table legends

Figure 1. Alphaproteobacteria commensals trigger qualitatively similar transcriptional responses in host roots.

(A) A principal coordinates analysis separated transcriptome of axenic roots (asterisks), roots inoculated with Rhizobiales commensals (closed shapes), and roots inoculated with sister lineage isolates (open shapes). (B) A heatmap showing cosine similarities between logFC upon Alphaproteobacteria commensal inoculations. (C) Heatmaps showing $\log_2$-scale count per million (log2cpm), zero-centered expression values, $\log_2$-scale fold changes (logFC), and significance (FDR < 0.05; |logFC| > 1), aligned according to their k-means cluster assignment (k = 9, based on Bayesian information criterion). (D) Boxplots showing logFC of each k-means cluster. Asterisks indicate statistical significance corresponding to Student's one-sample t test after Bonferroni's correction for multiple comparisons ($\mu = 0$; $\alpha = 0.001$) and letters indicate statistical significance corresponding to pairwise Wilcoxon's rank sum test after Bonferroni's correction for multiple comparisons within each cluster ($\alpha = 0.05$). (E) A heatmap showing enrichment of GO terms in the k-means clusters. (F) A network plot of enriched GO terms. Each node represents each GO term, and GOs with overlapping gene contents are connected with edges. k-means assignment of composing genes is shown as a pie chart. We selected the terms with the best P values from each of the 9 clusters, with the constraint that there are no more than 15 terms per cluster and no more than 250 terms in total. Representative terms are manually curated and indicated with composing k-means clusters for each GO cluster.

Figure 2. WRKY and ANAC transcription factors are important for transcriptional reprogramming.

(A) Heatmaps showing mean logFC of each cluster (left) and the enrichment of corresponding transcription factor binding motifs in their promoter regions (1-kb upstream from transcription initiation sites). AHL, AT-HOOK MOTIF CONTAINING

1138 NUCLEAR LOCALIZED; CCHC, CCHC-type zinc-finger motif containing protein;
1139 ATHB, ARABIDOPSIS THALIANA HOMEOBOX; FRS9, FAR1-RELATED
1140 SEQUENCE9. (B) GENIE3-inferred gene regulatory network using WRKY (green) and
1141 ANAC (magenta) family DETFs as potential regulators (colored; bigger node size).
1142 Arbitrarily defined modules are shown by dotted lines. (C) Degree, closeness, and
1143 betweenness centralities were computed based on the network in (B) for all potential
1144 regulators. Green and magenta dots correspond to WRKY and ANAC family TFs.
1145
1146 **Figure 3. Non-pathogenic microbial inoculation triggered similar transcriptional**
1147 **responses in the host roots.**
1148 (A) A heatmap showing cosine similarities between logFC upon different microbial
1149 inoculations. DEGs were selected based on the inoculation in rows (numbers of DEGs
1150 are shown in parentheses), whose logFC cosine similarity was calculated in
1151 comparison with inoculations in columns. For each row, all cosine similarity values
1152 were plotted on the right, whose colors indicate the lifestyle of the comparing
1153 inoculation. (B) Cosine similarities within non-pathogenic inoculations and within
1154 pathogenic inoculations were higher than those between pathogenic and non-
1155 pathogenic inoculations. (C) Principal coordinates analysis based on logFC cosine
1156 similarities of all commonly quantified genes (n = 21,815). Colors correspond to
1157 lifestyles. (D) Constrained analysis of principal coordinates (CAP) based on the logFC
1158 cosine similarities, using the constraining and conditioning factors indicated above.
1159 Colors correspond to inoculated microbial strains. (E) A heatmap showing logFC of
1160 genes assigned with the GO categories related to detoxification and response to
1161 hydrogen peroxide, reactive oxygen species, and hypoxia. Inoculations are aligned
1162 according to the dendrogram in (A) and genes are aligned according to k-means
1163 clustering as shown in Supplemental Figure 2B. Numbers indicated in the names of
1164 inoculation indicate the time point of harvesting (dpi).
1165
1166 **Figure 4. Rhizobiales-specific DEGs are potentially regulated by ANAC060.**
1167 (A) Heatmaps showing log2cpm, zero-centered expression values, logFC,
1168 significance, and GO assignment of genes specifically regulated by Rhizobiales
1169 commensals but not by sister lineage isolates. (B) Enlarged view of the GENIE3-
1170 inferred GRN, shown in Figure 2B, colored for potential regulator TFs (left) or

1171 Rhizobiales-specific DEGs (right). (C) Same view as in (B), colored by their logFC
1172 upon different bacterial inoculation.
1173
1174 **Figure 5. Plant sulfated peptide pathway is needed for R129_E RGP activity.**
1175 (A) Primary root growth and representative pictures of Col-0 and *tpst* plants grown
1176 axenically or inoculated with R129_E. Seeds were inoculated and grown under
1177 continuous light conditions for 12 days. (B) Bacterial abundance relative to plant
1178 biomass was quantified by DNA-based quantitative PCR using primers specific to *A.*
1179 *thaliana* and R129_E *16S rRNA* genes. No clear depletion of bacterial cells from *tpst*
1180 roots was observed. (C) Mutants impaired RGF1 perception (*rgi1;2,3;4;5-1*) or PSK
1181 perception (*pskr1pskr2psy1r*) did not phenocopy *tpst* when 7-day-old seedlings were
1182 inoculated with R129_E for 14 days under short-day conditions. (D) Col-0 root MZ
1183 accumulate higher amounts of proPLT1::PLT1-GFP when 7-day-old seedlings were
1184 inoculated with R129_E for 7 days under short-day conditions, whereas *tpst* root MZ
1185 accumulated a similar amount irrespective of R129_E inoculation. For each panel, a
1186 merged image of propidium iodide staining (gray) and PLT1-GFP (green) signals and
1187 an image only showing PLT1-GFP signals pseudo-colored as shown in the calibration
1188 bar are shown in left and right, respectively. Bars indicate 50 μm. Images are aligned
1189 with quiescent centers on the dotted line. Letters indicate statistical significance (α =
1190 0.05) corresponding to Student's *t* test after fitting to a linear mixed model with
1191 biological and technical replicates as random factors, corrected for multiple
1192 comparison by the Benjamini-Hochberg method.
1193
1194 **Figure 6. TPST is needed for the RGP activity explicitly exerted by Rhizobiales**
1195 **RGP but not Pseudomonadales.**
1196 Seven-day-old seedling of Col-0 and *tpst* were inoculated with a panel of Rhizobiales
1197 commensals (A) or Pseudomonadales commensals (B) and grown for 14 days under
1198 short-day conditions. Letters indicate statistical significance (α = 0.05) corresponding
1199 to Student's t test after fitting to a linear mixed model with biological and technical
1200 replicates as random factors, corrected for multiple comparison by the Benjamini-
1201 Hochberg method.
1202
1203 **Supplemental Figure 1. Qualitative comparison of DEGs for**
1204 **Alphaproteobacteria inoculations**

1205 Upset diagrams showing the number of DEGs specific to or shared (intersect) between
1206 different inoculations. Up-regulated and down-regulated DEGs were separately
1207 analyzed.
1208
1209 **Supplemental Figure 2. Similarity in gene contents between GO categories**
1210 **enriched in Alphaproteobacteria DEGs based on *k*-means clustering.**
1211 For each cluster, significant enriched GO categories are shown in rows. Genes in the
1212 respective clusters with at least one significantly enriched GO category are shown in
1213 columns. Assignment of a gene to a given GO category is indicated by black filling
1214 color. GO categories with highly similar gene contents are manually marked and
1215 representative terms are indicated. Bold R and B in the labels indicate "response to"
1216 and "biosynthesis of", respectively.
1217
1218 **Supplemental Figure 3. WRKY54 and ANAC060 are associated with responses**
1219 **characteristic to sister lineage and Rhizobiales isolates, respectively.**
1220 The same GRN as in Figure 2B, colored by k-means clusters (A), by logFC upon
1221 Alphaproteobacteria commensals (B; the full view of Figure 3C), and for Rhizobiales-
1222 specific DEGs (C; the full view of Figure 3B). Module 1 and 2 contain genes from
1223 Clusters 1, 8, and 9 and Clusters 3, 4, and 6, respectively, and Rhizobiales DEGs
1224 were exclusively found in the module 2. Part of the network presented in Figures 4B
1225 and 4C are indicated by a square.
1226
1227 **Supplemental Figure 4. Robust centrality of WRKY54 and ANAC060 irrespective**
1228 **of the lists of potential regulators.**
1229 GENIE3-based inference of gene regulatory network using all differentially expressed
1230 transcription factors as potential regulators, colored for transcription factor families (A),
1231 by k-means clusters, corresponding to Figure 1B (B), for Rhizobiales-specific DEGs,
1232 corresponding to Figure 3A (C) or by logFC (D). Modules are arbitrarily defined. (E)
1233 Centrality indices of potential regulators in the inferred GRN.
1234
1235
1236 **Supplemental Figure 5. Non-pathogenic microbial inoculation triggered similar**
1237 **transcriptional responses in the host roots.**

1238 (A) A heatmap showing logFC of genes differentially expressed at least in one of the
1239 analyzed treatments (n = 13,889), aligned according to *k*-means clustering (*k* = 21,
1240 based on Bayesian information criterion). Assignment of genes to *k*-means cluster for
1241 Alphaproteobacteria dataset (Figure 1) are also shown above. (B) GO enrichment
1242 analysis of k-means clustering shown in (A), as in Figure 1F. (C) A heatmap showing
1243 logFC of GST genes, aligned according to their phylogeny. Shaded by blue are the
1244 genes specifically acquired within the family Brassicaceae (Pisléska-Bednarek et al.,
1245 2018).
1246
1247 **Supplemental Figure 6. ANAC060 is expressed in the cell population within the**
1248 **root meristematic zone, where PLETHORA TFs and RGF peptides are also**
1249 **expressed to control meristematic mitotic activity.**
1250 (A) T-distributed stochastic neighbor embedding (t-SNE) of single cell RNAseq
1251 datasets reported by Denyer and Me et al. (2019), where colors correspond to the
1252 normalized expression levels of genes indicated above. (B) Cluster assignment of
1253 ANAC060, PLT1, PLT2, and PLT4, where the cluster 11 corresponds to the
1254 meristematic cell population. t-SNE and violin plots were created by The Plant Single
1255 Cell RNA-Sequencing Database. (C) GO enrichment analysis of 100 genes best co-
1256 expressed with ANAC060 in the single cell RNAseq datasets, based on Pearson's
1257 correlation-based Mutual Ranks. Data are visualized as in Figure 1F.
1258
1259 **Supplemental Figure 7. DNA synthesis and auxin and cytokinin accumulation in**
1260 **axenic and R129_E-inoculated roots.**
1261 (A) Roots incubated with EdU for 2 hours were staining with Alexa488 after seeds
1262 were inoculated with R129_E for 21 days under short-day conditions. EdU/Alexa488
1263 signals in green was merged with autofluorescence signals in magenta. (B) Roots
1264 expressing DR5:ER-GFP were imaged after seeds were inoculated with R129_E for
1265 8 days under short-day condition. (C) Roots expressing TSCn:ER-GFP were imaged
1266 after 7-day-old seedlings were inoculated with R129_E for 10 days under short-day
1267 conditions. Bars, 50 μm.
1268
1269 **Supplemental Figure 8. RGF and CIF peptide pathways were not essential for**
1270 **R129_E RGP activity.**

1271 (A) R129_E promoted primary root growth of Col-0, *rgf123*, and *sgn3* plants after 7-
1272 day-old seedlings were inoculated for 14 days under short-day conditions. (B) External
1273 application of 100 nM RGF1 or 100 nM desulfated RGF1 did not affect the ability of
1274 R129_E to promote root growth of Col-0 and did not rescue the lack of RGP in *tpst*
1275 mutant roots. Letters indicate statistical significance (α = 0.05) corresponding to
1276 Student's *t* test after fitting to a linear mixed model with biological and technical
1277 replicates as random factors, corrected for multiple comparison by the Benjamini-
1278 Hochberg method. (C) Roots of *tpst* mutant plants were stained with 10 μg/mL
1279 propidium iodide after 7-day-old seedlings were inoculated with R129_E for 14 days
1280 in the presence or absence of 100 nM RGF1. Arrowheads indicate the site of transition
1281 from cell division to cell elongation. Bars, 50 μm.
1282
1283 **Supplemental Table 1. RNAseq datasets analyzed in this study.**
1284 **Supplemental Table 2. Pairwise PERMANOVA of logFC by lifestyles**